Sensing in Everting Vine Robots

Allison Raines

A thesis
submitted in partial fulfillment of the
requirements for the degree of

Master of Science in Engineering

University of Washington

2022

Reading Committee:
Blake Hannaford, Chair
Chet Moritz

Program Authorized to Offer Degree:
Electrical and Computer Engineering

University of Washington

Abstract

Sensing in Everting Vine Robots

Allison Raines

Chair of the Supervisory Committee:
Professor Blake Hannaford
Electrical Engineering

Acoustic signals can be used to detect environmental interactions of everting tube robots. The experiments in this thesis distinguish differences in pressure and audio signals in tubes freely everting through different-sized tunnels, with acoustic signal measurement ranging from 0-10 kHz. Pressure rises when transitioning to smaller tunnels and drops when transitioning to larger tunnels. Audio becomes louder when transitioning to larger tunnels and quieter when transitioning to smaller tunnels. Audio FFTs and spectrograms also show distinguishable eversion sounds and clear evidence of tunnel transitions. Time data suggests that reliable time series models could be created to detect tunnel transitions. Frequency data also suggests that a reliable spectral analysis model could be created to detect tunnel transitions. In practice, these findings could be used to deploy everting tubes as sensors in hard-to-reach places. In medical environments that are not easily seen and are not safe for rigid probes, such as the mammary glands, brain ventricles, the trachea and the colon, acoustic sensing can help indicate what the environment looks like and if the tube is maneuvering properly.

TABLE OF CONTENTS

LIST OF FIGURES

GLOSSARY

ENTERING CONSTRICTION (TR1) TRANSITION: A term, abbreviated to (TR1), to concisely reference the transition of an everting tube from a tunnel with a larger cross-sectional area to a tunnel or constriction with a significantly smaller cross-sectional area. The order of events is indicated by '1'. The everting tube first enters a constriction (TR1) and then exits (TR2).

EXITING CONSTRICTION (TR2) TRANSITION: A term, abbreviated to (TR2), to concisely reference the transition of an everting tube from a tunnel or constriction with a significantly smaller cross-sectional area to a tunnel with a larger cross-sectional area. The order of events is indicated by '2'. The everting tube first enters a constriction (TR1) and then exits (TR2).

EVERSION: A method of growth via tip extension, all new material is pulled from within the tip to lengthen the body.

FREE EVERSION: Pressure within the system is set above the yield threshold of the system [5] with sufficient pressure to grow throughout the entire tunnel. Growth is not limited by actuation or friction at the reel.

LARGER-TO-SMALLER (LS) TRANSITION: A term, abbreviated to (LS), to concisely reference the transition of an everting tube from a tunnel with a larger cross-sectional area to a tunnel with a smaller cross-sectional area.

SMALLER-TO-LARGER (SL) TRANSITION: A term, abbreviated to (SL), to concisely reference the transition of an everting tube from a tunnel with a smaller cross-sectional area to a tunnel with a larger cross-sectional area.

ACKNOWLEDGMENTS

The author wishes to express sincere appreciation to her advisor, Blake Hannaford, for his constant guidance and wisdom, and for making this project possible. Sincere gratitude is extended to Andrew Lewis and Joel Hwee for their invaluable help and for showing the ropes of eversion. Appreciation is also extended to Yana Sosnovskaya, Gray Hooper and Cindy Imm for their work supporting this project. This work was made possible by the U.S. Air Force Graduate program, the Paul C. Leach Fellowship with the UW Electrical and Computer Engineering Department, as well as the UW Veterans Education Benefits office.

DEDICATION

to my Lord and Savior, Jesus Christ, and my family.

Chapter 1

INTRODUCTION

1.1 Background

Everted tubes are a type of soft robot that grow from the tip like a vine (Fig. 1.1). The robot body is often made of a lightweight, flexible plastic material and stored on a reel within a pressure vessel [5, 6]. Eversion is where a tube pneumatically inflates, growing from pressure forces at the tip that pull material through its interior. Growth extends in the direction of least resistance, enabling it to explore complex environments [5]. Because of this internal feed of material, it does not slide against the environment as it grows and thus applies minimal friction and forces on its environment, which may be valuable for sensitive medical applications [4]. This lack of sliding decreases insertion forces and prevents it from dispersing bacteria along lumens like the urethra [7, 8].

This experiment uses freely everting tubes but other everting tubes may be controlled by motors [1] or steered by integrated actuators [9]. The dynamics of everting tube growth are nonlinear which has made mathematical modeling difficult [5], but sensory capabilities from this study may be used to improve control techniques.

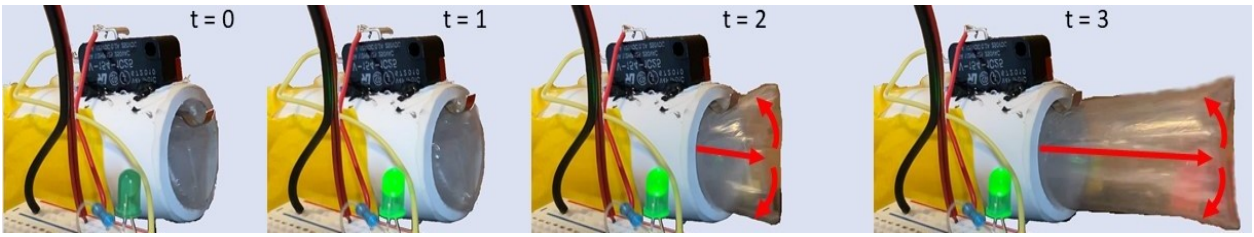

Figure 1.1: Example of everting tube emerging from a pipe (tunnel). Limit switch and LED record the event.

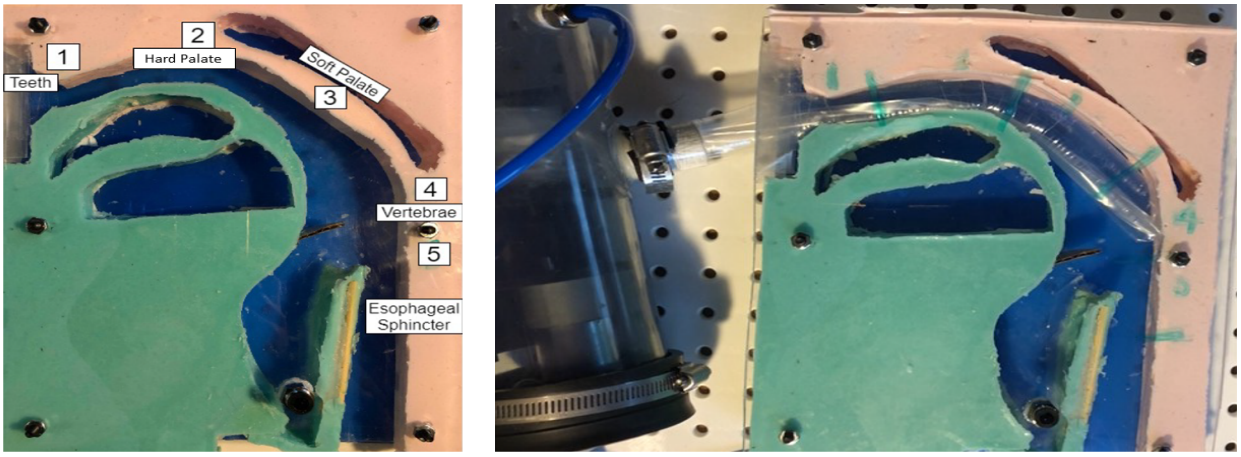

Figure 1.2: Airway management application sends everting tubes into airway phantom. From "An Everting Emergency Airway Device" paper [1].

Everting robots are useful in medical applications because they have minimal impact on their environment and can get to hard-to-reach places. One application is emergency airway management. Recent research investigates sending multi-material everting tubes into the trachea to seal the airway and restore oxygenation in sub/unconscious patients (Figure 1.2). The everting tube passively navigates the airway but has no sensing feedback. Other applications send everting tubes into the large intestine in colonoscopies, into mammary glands in breast cancer detection, and into brain ventricles in brain surgery (Figures 1.3, 1.4, 1.5). But, none of these applications use sensing to make environmental inferences.

There is growing interest in adding actuation and sensing elements to the body and tip of everting tubes. Though many applications may require information about environmental interactions, adding sensors to the tubing body may be disadvantageous. Researchers have deployed camera sensors at the tip of everting tubes. The camera is held in place by a cable running through the body of the robot [5] but the presence of delicate sensors like this may introduce safety or reliability issues. This paper introduces the use of pressure and audio signals detected at the base of the everting robot in order to infer transient changes in the environment in the everting tube.

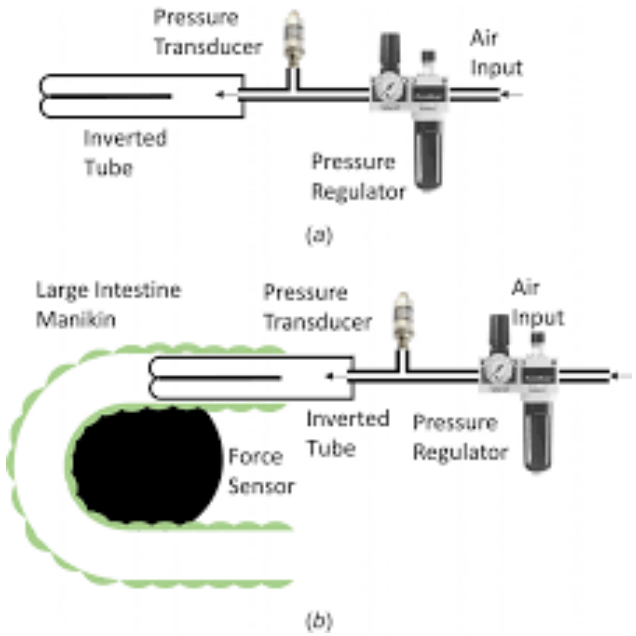

Figure 1.3: Colonoscopy application sends everting tubes into large intestine (diagram). From "Tubular Locomotion and Positioning Using Tip Eversion for Endoscopy" paper [2].

1.2 Related Work

Our study is the first of its kind to investigate acoustic signals within everting tubes. There are studies that test resonance theory of ultrasonic scattering in elastic spheres [10]. There has also been audible-range communication at a distance used in cylindrical multi-robot systems [11]. But, no eversion studies look at audible-range acoustic signals within the inflated everted tube as a means of understanding the configurations of the robot or its environmental interactions. The first literature review of everting robots (2017)[5] establishes basic everting pressure properties, such as smaller gaps requiring higher pressure to evert through, but it does not cover these interactions over time. MAMMOBOT, a millimeter scale steerable soft robot, used pressure within the tube to build a dynamic model for breast cancer detection but does not infer much about the environment [3]. The experiments described below are the first to characterize audible range signals within the robot and use them to

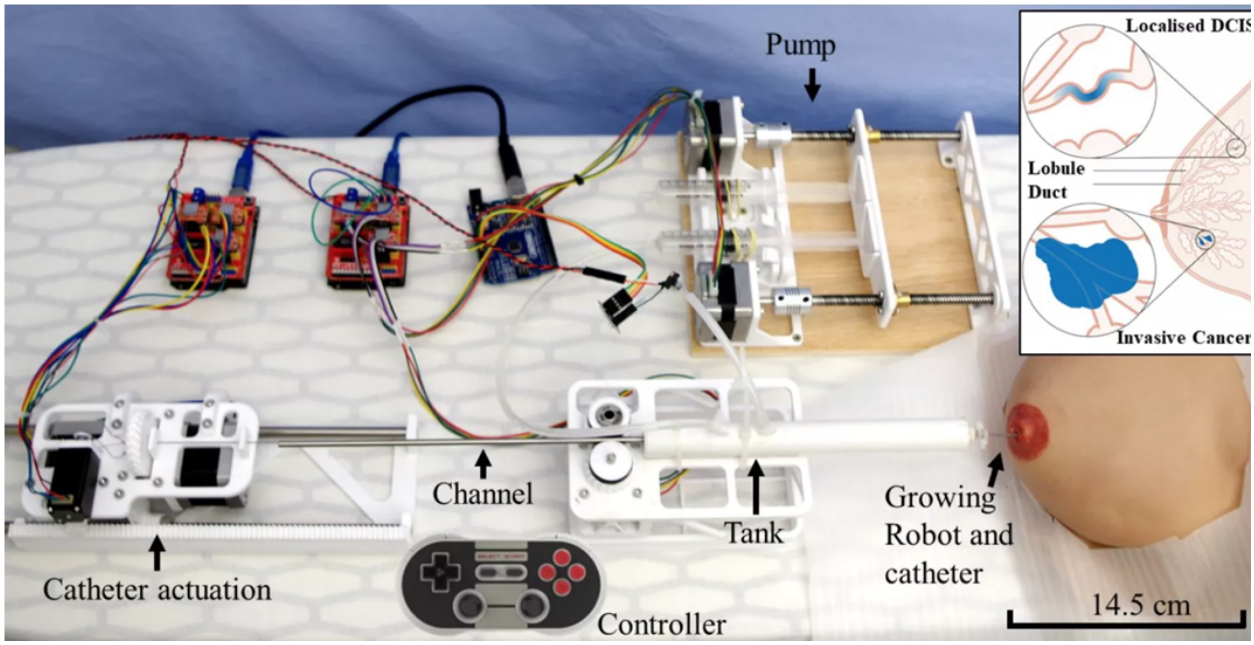

Figure 1.4: Breast cancer application sends everting tubes into mammary gland phantom. From "MAMMOBOT: A Miniature Steerable Soft Growing Robot for Early Breast Cancer Detection" paper [3].

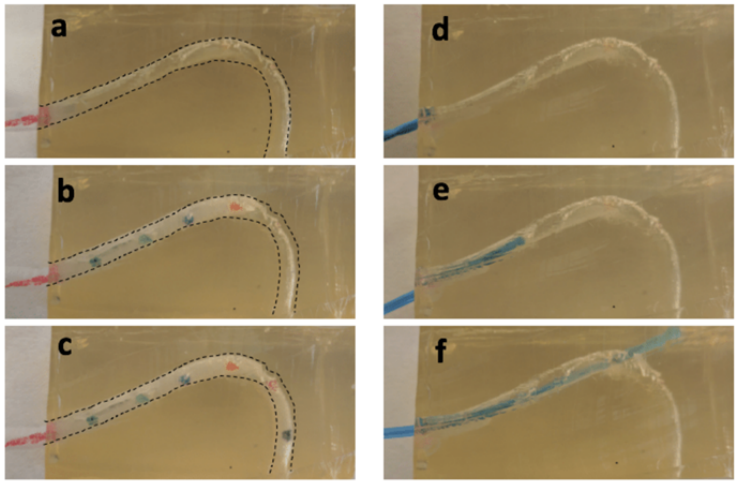

Figure 1.5: Brain surgery application sends everting tubes into brain ventricle phantom (Compared to standard catheter). Soft catheter: (a) at entry point, (b) prior to 90 degree bend, (c) at drainage point. Standard catheter: (d) at entry point, (e) prior to 90 degree bend, (f) unsuccessful in achieving 90 degree bend. Labels and figure from "Design of a soft catheter for low-force and constrained surgery" paper [4].

infer characteristics about the environment relative to the everting tube.

Everting tubes are being studied and applied in medical procedures within mammary glands, brain ventricles, the trachea and the colon [3, 4, 1, 2]. These body orifices are tunnel-type environments, and this study looks at sensing in similar tunnel environments.

1.3 This Thesis

Sensing the growth characteristics in real time with simple and unobtrusive sensors would be useful to the theory and applications of everting tubes. By indicating configurations of the robot and environmental interactions, the robot could be better controlled or used as a sensor in hard-to-reach places.

In this paper, we present eversion pressure and acoustic signals identified through (1) post-processing algorithms related to tunnel transitions and (2) spectrum analysis distinguishing specific eversion mechanism sounds. Section II describes the everting robot and experimental setup. In Section III, the eversion signals recorded during eversion experiments are presented. In Section IV, the algorithms that are used to identify transitions are evaluated and the eversion sound spectra are characterized. Limitations and concluding remarks are discussed in Section V.

The novel contributions of this thesis are as follows:

- The first study of its kind to investigate pressure and audio signals within everting tubes.

- A means of detecting internal signal responses and distinguishing spectrogram characteristics for everting tubes.

- A peer reviewed paper titled “Inferring Environmental Interactions of Soft Everting Robots From Acoustic Signals” has been submitted to the International Conference on Intelligent Robots and Systems (IROS)

Chapter 2

ALTERNATING TUNNELS EXPERIMENT

2.1 Introduction

This experiment sends an everting tube through a series of different-diameter tunnels and gathers internal pressure and audio signals. From the eversion growth model of [5], it is known that a different pressure is required to grow everted tubing different diameters. We are interested in growing into tunnels of different diameters and so we hypothesize that different pressures would also be required. It is hypothesized that pressure signals will rise in smaller tunnels and fall in larger tunnels since pressure must build to pass though smaller tunnels. This build up of pressure takes time and as it grows slower in smaller tunnels, there will be less plastic crinlking and eversion sounds. So, audio amplitudes can be hypothesized to be lower. As it grows faster in larger tunnels, audio amplitudes can be hypothesized to be higher.

2.2 Methods

In order to investigate the transient and steady-state effects of tunnel diameter transitions on an everting tube's internal pressure and audio, a Low-Density Polyethylene (LDPE) tube was freely everted into a tunnel of varying sizes while pressure and audio signals were captured. Free eversion means that pressure within the system was set above the yield threshold of the system [5] with sufficient pressure to grow throughout the entire tunnel and growth was not limited by actuation or mechanical friction. A transition refers to the passage of the everting tube from tunnel to the next and, sampling transitions, a total of 40 samples were collected (4 transitions per trial x 11 trials = 22 Larger-to-Smaller (LS) tunnel diameter transitions and 22 Smaller-to-Larger (SL) transitions).

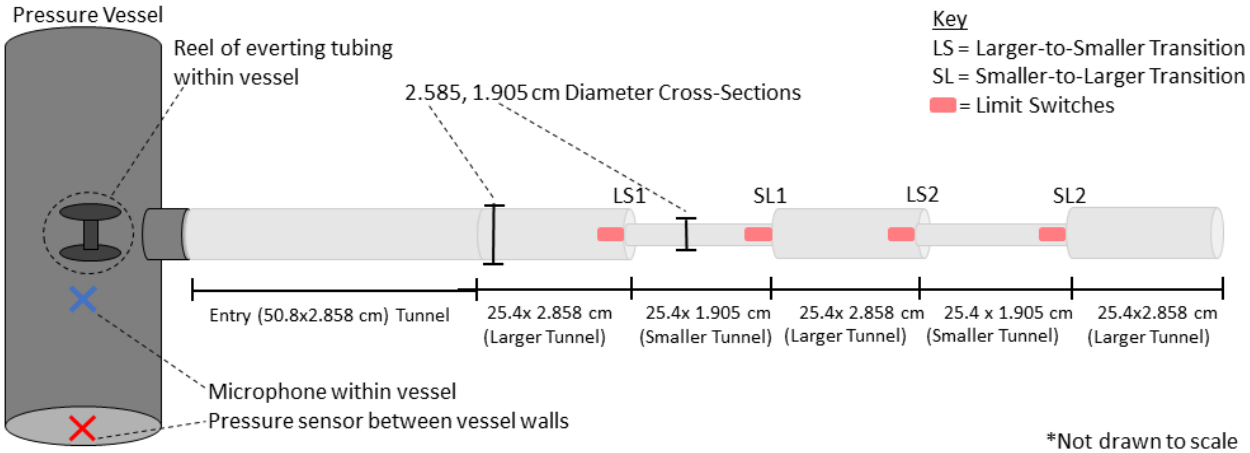

Figure 2.1: Experimental Setup (Full Tunnel Test). Opening of pressure vessel sends everting tube directly into tunnels.

2.2.1 Soft Everting Robot

LDPE (Uline #S-3521) tubing with 3.81 cm flat width and 2mil (0.05mm) wall thickness was used as the everting material. The tubing takes on a 2.858 cm diameter when fully inflated to 3 PSI.

2.2.2 Tunnel and Switches

An everting tube was grown into a multi-section tunnel composed of PVC pipe (Fig. 2.1, 2.4). The experiment tunnel (50.8 cm long with a 2.858 cm internal diameter (50.8 cm x 2.858 cm)) begins with an entry tunnel, which gives space for growth of the free everting tube to stabilize and for pressure to build up to the standard everting pressure of the larger tunnel ($\tilde{2}$ psi). The entry tunnel was followed by 5 alternating-sized sections (larger 25.4 cm x 2.585 cm and smaller 25.4 cm x 1.905 cm (length x internal diameter)).

To detect transitions, limit switch arms were carefully positioned at the end of each alternating section, detecting two larger-to-smaller (LS) and two smaller-to-larger (SL) tunnel transitions per trial. Limit switches were positioned such that passage through the diameter

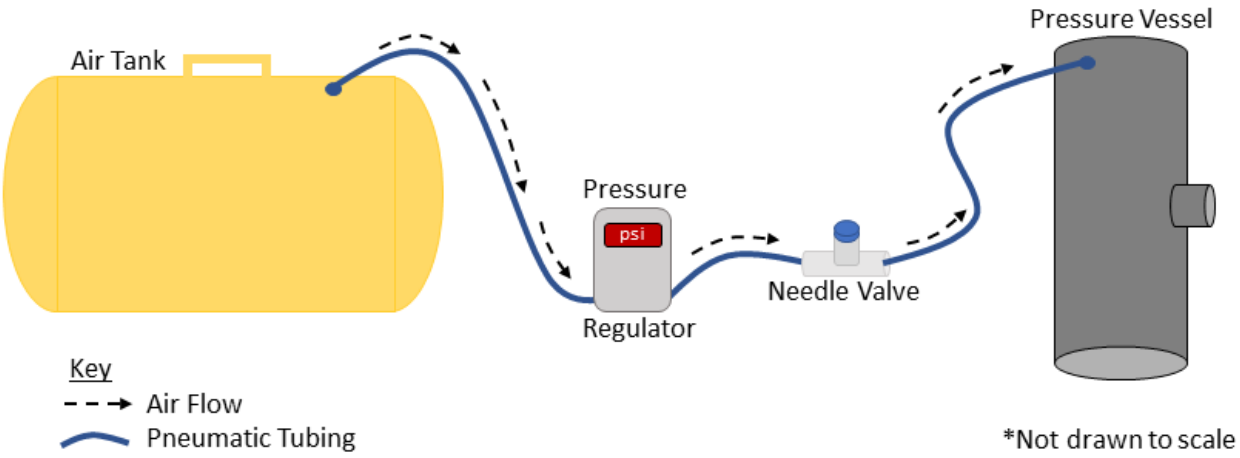

Figure 2.2: Pneumatic Circuit. Air flowing left to right. Air tank serves as capacitor. Pressure regulator and needle valve regulate constant air flow to pressure vessel.

transition events was detected within ±38.1 ms accuracy as read by an Arduino Uno. The limit switch was aligned by hand using slow motion video segments (Fig. 1.1). This placement was measured and replicated for the remaining tunnel segments. Limit switch error was quantified based on: (1) Measurement error in cutting the tunnels and switch placement (x = ± 0.11 cm total), which, at the average velocity (v) of the trials and taking into account the average time between Arduino sample (± 1415 us), corresponds to a time accuracy ($\frac{x}{v}$ = ± 4.8 ms). (2) Time accuracy between video frames was used to place the switch (frame rate accuracy ± 33.33 ms). Therefore, $\frac{x}{v}$+ frame rate accuracy = ± 38.1 ms total. The switches were covered with a dot of hot glue at the tip of the arm to keep it from puncturing the everting tube. The actuation force was negligible and had no visible impact on the pressure signal. A click from switch actuation was detectable in the audio recording.

2.2.3 Air Supply

A 10 lb air tank was connected to a proportional controlled pressure regulator (SMC Electro-Pneumatic (E/P) regulator ITV2011-04N2N4) to supply stable input pressure to a needle

valve that was locked in position to create a steady flow of 900 cm^3/s into the pressure vessel at the everting tube base (Figure 2.2 and 2.4). This flow rate was estimated from a video of an everting tube growing alongside an imperial ruler (converted to metric) as seen in Figure 2.3. Using two reference points for pressure (P) and volume(V), the difference in cylindrical volume was found and Boyle's law was applied, $P_1V_1 = P_2V_2$.

2.2.4 Sensors

A pair of sensors in the pressure vessel collected a full spectrum of pressure signals, accurate from 0 to 10 kHz. Specifically, a board-mount differential pressure sensor (Honeywell SSC-DANN150PG2A3) was used with a resolution of 0.01 psi through serial communication on an Arduino Uno at 660 Hz. An I2S digital MEMs microphone (Knowles SPH0645LM4H-B) was sampled by a Raspberry Pi microcomputer board at 48 kHz. At set-up, the Arduino sent a one-second digital output pulse to the microphone. This pulse was visible on the audio signal and allowed the Arduino and Raspberry Pi data to be synced. The microphone was placed directly in the vessel and the pressure sensor was placed between the walls of the vessel, with one port reading internal vessel pressure and the other reading room pressure.

2.2.5 Filtering and Windowing

Audio (microphone sensor data) was Hamming windowed to help reduce DC component at 0 Hz and high-pass filtered to remove frequencies detected by the pressure sensor. A 140 Hz low-pass filter (LPF) was applied on the pressure data, and a 140 Hz high-pass filter (HPF) was applied on the audio data. This ensured accurate, full spectrum collection based on the following considerations: 1) 140 Hz LPF cutoff is almost a factor of 5 below the pressure sensor's sampling rate, and 2) 95% of the pressure signal's energy was calculated to lie below 140 Hz. 3) In the microphone's datasheet, the frequency response performance curve starts to roll off below 100-200 Hz and above 10 kHz. The 95% window of audio energy was calculated to lie below 8155 Hz.

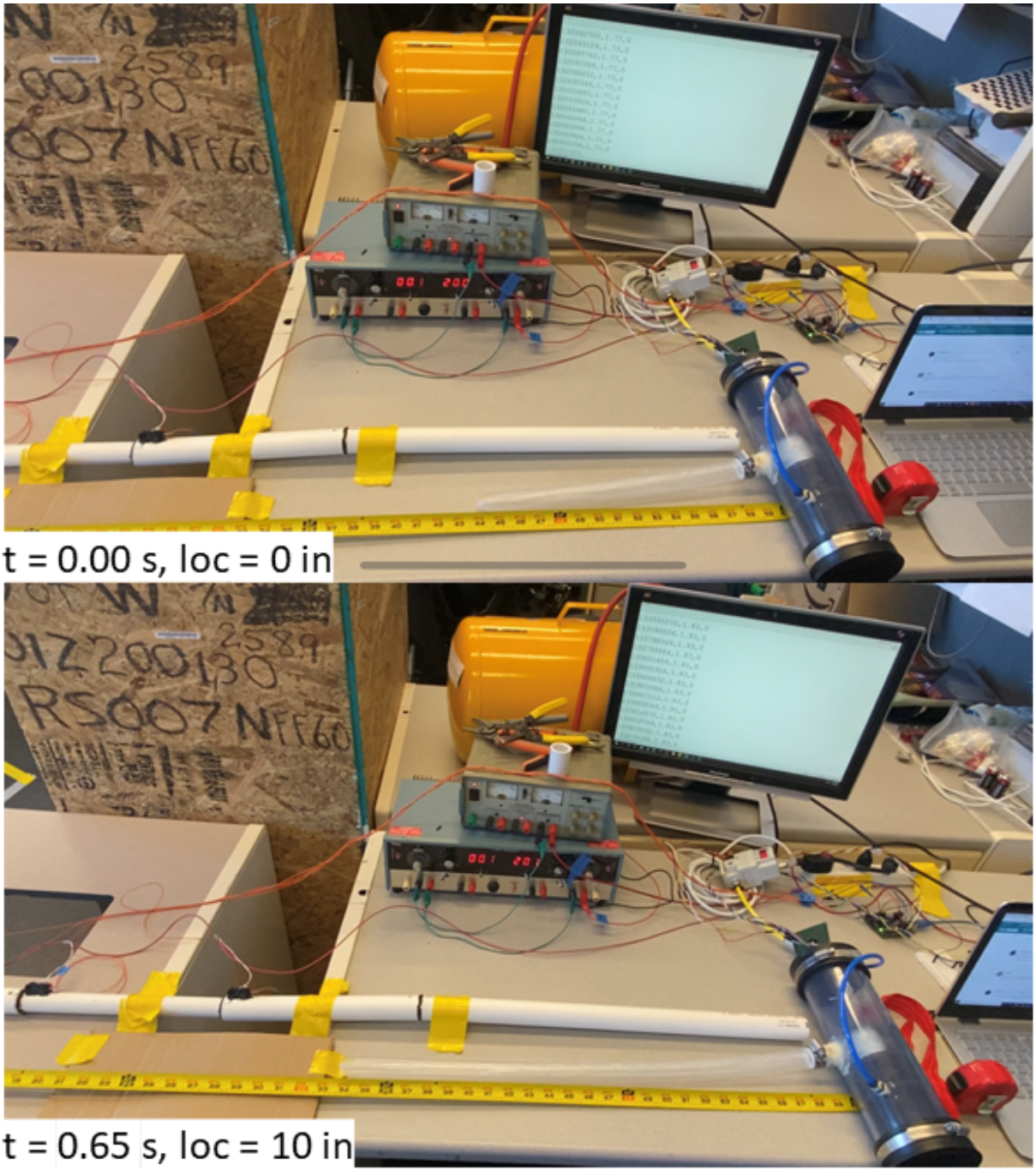

Figure 2.3: Flow Rate Video Frame Analysis. Video frames spanning 0.65 s and 25.4 cm used in flow rate calculations.

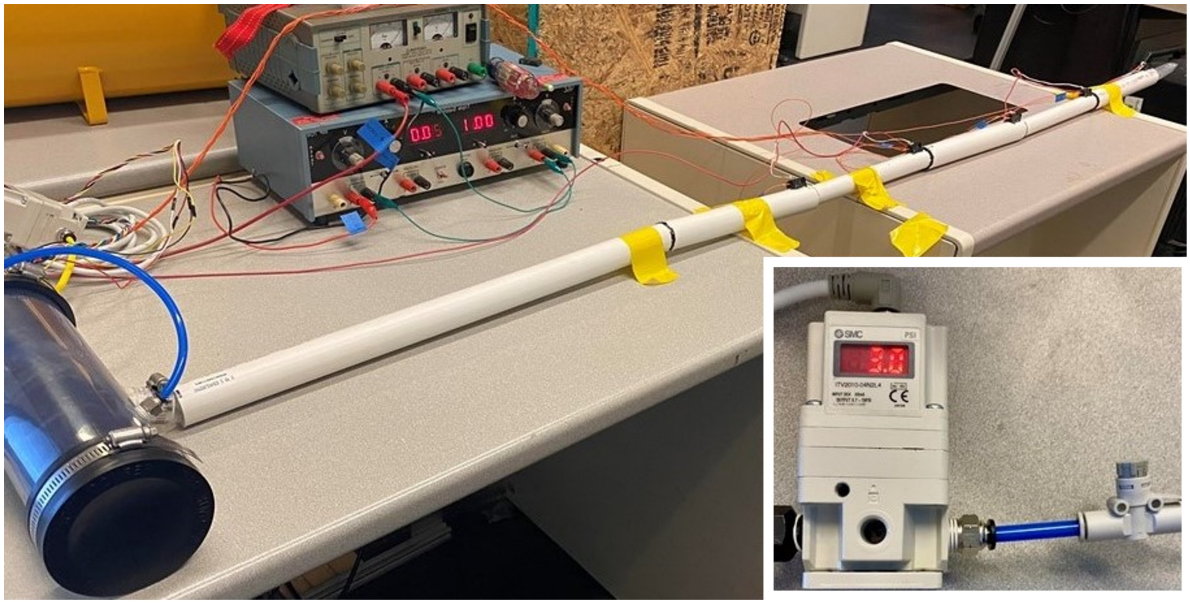

Figure 2.4: Desktop Setup (Full Tunnel Test) *Foreground*: Pressure vessel, tunnels. Background: Yellow air tank, power supplies. *Bottom right*: Pressure regulator, needle valve.

2.2.6 Sound Classification

Sounds during eversion arise from multiple sources within the system, such as plastic crinkling from the tubing and air flow into the pressure vessel. We isolated and sampled these sounds. Using the microphone, we sampled isolated eversion sounds unique to our set-up. These sounds were analyzed using Fast Fourier Transforms (FFTs) and spectrograms to identify characteristics unique to each. We will discuss how we captured four of these sounds in isolation: *Switch Clicked*, *Friction of Reel*, *Air Inflow* and *Eversion into Tunnel*.

Switch Clicked: The switch was pressed, but not released because the everting tube was continuously pressurized during the experiment. *Friction of Reel*: A string was wound onto to the reel and pulled out the mouth of the pressure vessel. The string was hand-pulled at an approximately constant rate of 25.4 cm/s. *Air Inflow*: The air supply delivered the constant $\tilde{9}00$ cm^3/s of air into the pressure vessel. To approximate eversion pressure build-up, a piece of duct tape with a small hole covered the pressure vessel's mouth. This may

have increased the frequency and sound level. This airflow was supplied by the air tank, E/P regulator, and needle valve. The E/P regulator's internal solenoid valve produces humming sounds, but since it was outside the enclosed vessel and tunnels, the humming sounds was minimally present in this recording. *Eversion into Tunnel*: A short length of LDPE was inserted directly into the pressure vessel, without being rolled onto a reel. The vessel was pressurized with a constant flow, and the everting tube grew into a 25.4 cm section of the 2.858 cm larger tunnel. Note that sounds of airflow were still present, as airflow and eversion are inherently linked.

2.2.7 Thresholding Algorithms

Tunnel transitions were estimated based on the rise and fall of pressure and audio data. To do so, we programmed two offline thresholding algorithms for pressure and audio time domain signals. The pressure thresholding algorithm analyzes one transition at a time. First, before thresholding, a Butterworth filter and low pass filter is applied to the pressure signal. The algorithm then calculates a threshold which is used for the entire signal from an average of pressure samples from the last four tunnels (two upper limits and two lower limits). The upper limit is the 95th percentile of the everting pressure in the smaller tunnels (to eliminate outliers). The lower limit is the minimum everting pressure in the larger tunnels (the LS transition occurs quickly, reaches the lower pressure limit and immediately rises, so a 95th percentile is not applicable). Using this threshold, the algorithm finds the initial moment the filtered signal crosses a threshold. The audio thresholding algorithm analyzes one transition at a time. It takes the magnitude of the signal and detects transient peaks above a threshold. In an LS transition, the algorithm finds the last peak and declares a threshold crossing. Similarly, in an SL transition, the algorithm finds the first peak and declares a threshold crossing. Across all samples, the threshold was manually placed at 0.48 <unitless> to minimize time delays between the switch transition and the threshold crossing.

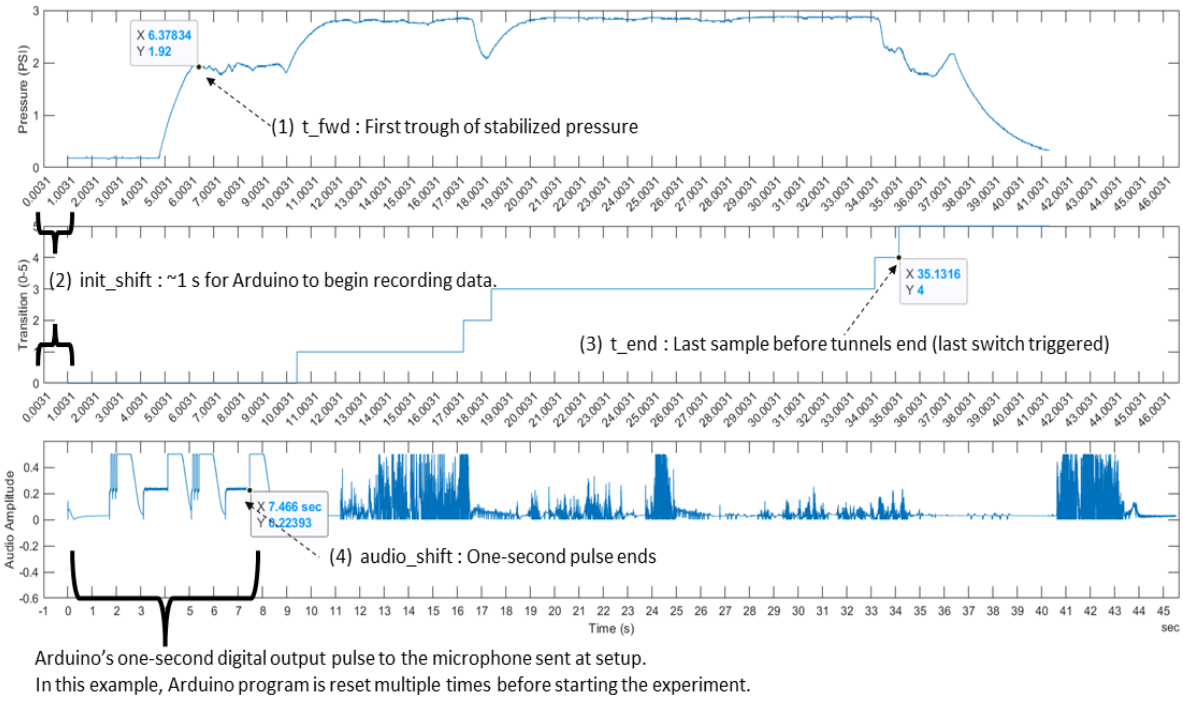

Figure 2.5: Raw Signals Manually Trimmed. Manually selected data points to trim and align signals. Top signal: Pressure (psi). Middle signal: Switch transitions indicated by 0-5. Bottom signal: Audio (unitless)

2.2.8 Signal Trimming

Signals were trimmed or "cropped" to cover events of interest (Fig. 2.5). For example, at "setup", the experiment first began when airflow was turned on and pressure began building from ambient room pressure. Once the everting tube navigated all tunnel transitions, the airflow was turned off and air pressure released for "tear down". Pressure and audio signals from these "set-up" and "tear down" events were not analyzed and were excluded from the displayed signals in this paper.

Four data points were manually gathered to trim signals and synchronize data from

the Arduino and Raspberry Pi. Figure 2.5 displays these data points and the resulting, trimmed signals are showed in Figure 2.6. The data points: 1) *t_fwd* was the first trough of stabilized pressure. At this point, based on the switch data, the everting tube was within the entry tunnel before the first larger tunnel section (25.4 cmx2.858 cm). 2) *init_shift* was the Arduino's initialization time lapse. The Arduino initialized and did not beginning recording data until ∼1 s in time. In this specific example in Fig. 2.5, there was a 1.0031 s gap at the start of pressure and transition data. 3) *time_end* was the last sample before the last switch is triggered at end of the tunnels. 4) *audio_shift* forward shifts the audio data based on a one-second digital output pulse from the Arduino. This shift synchronizes the Arduino and Raspberry Pi data.

The samples were indexed start to finish, (*time_start* : *time_end*), according to the following equations:

Pressure and switch data recorded by the Arduino:

$$time\_start = t\_fwd + init\_shift \tag{2.1}$$

$$time\_end = t\_end + init\_shift. \tag{2.2}$$

Audio data recorded by the Raspberry pi :

$$time\_start = t\_fwd + audio\_shift \tag{2.3}$$

$$time\_end = t\_end + audio\_shift \tag{2.4}$$

2.2.9 Spectrograms

Spectrograms and FFTs were generated from trimmed time domain signals. The exact duration of these signals varied slightly, since an input sample length which is a product of prime factors of the sampling rate (48 kHz) is optimal for Matlab's fft() function.

2.3 Results

A single selected trial will be discussed throughout the results section and in Figures 2.6, 2.7, 2.8 and 2.10 . However, the results hold for all other trials.

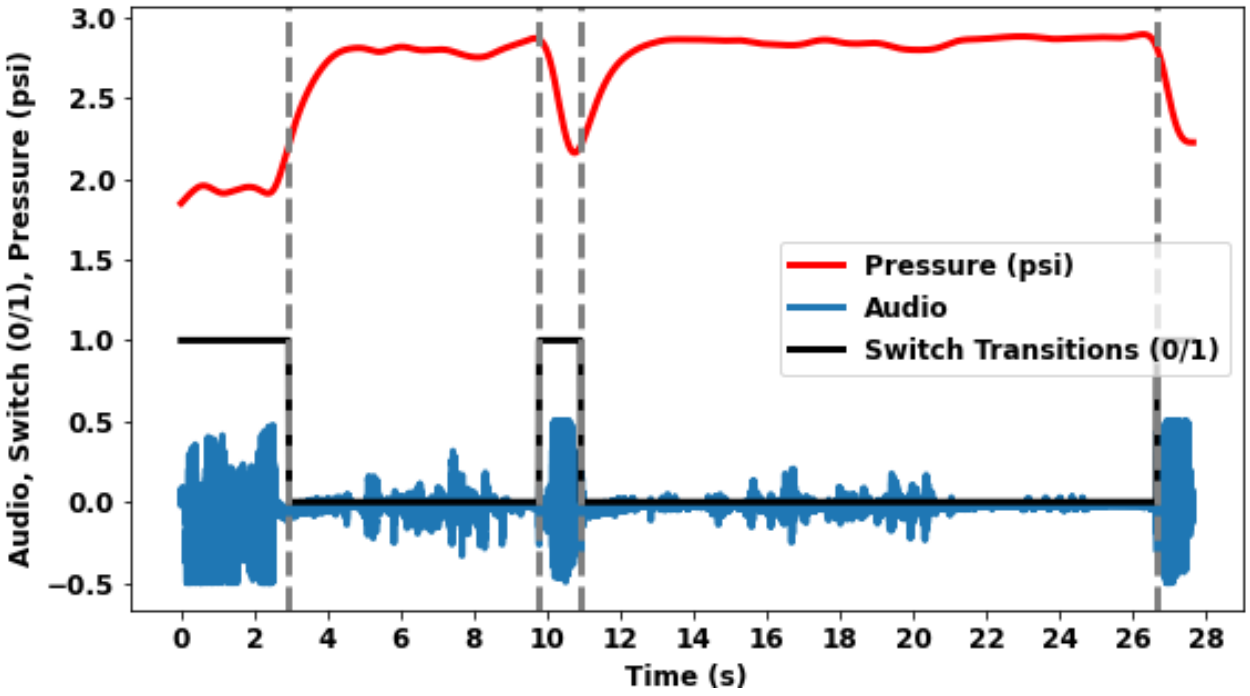

Figure 2.6: Pressure and audio transients. *Top*: Pressure signal (red, butterworth filtered) falls, holding 2 PSI in larger tunnel, and rises, holding 3 PSI in smaller tunnel. *Bottom*: Audio signal (blue) overlaid with limit switch data (black) approximating tunnel transitions.

In this sample trial, everting pressure is ∼2 psi in the larger tunnel and ∼3 psi in the smaller tunnel (Fig 2.6). The audio is around 0.5 <unitless> peak-to-peak in the larger tunnel and 0.1 peak-to-peak in the smaller tunnel. The limit switch signal (black) indicates tubing diameter (1 = large, 0 = small). This switch data was originally recorded as 0-5 (reference raw data in Fig. 2.5) but was converted to binary 0/1. An LS transition is indicated by 1 to 0 (1→0) and an SL transition is indicated by a 0 to 1 (0→1). In an LS transition (1→0), pressure rises over time to the everting pressure of the smaller tunnel. In an SL transition (0→1), pressure drops (∼3→2 psi) from the smaller tunnel's everting pressure to larger tunnel's everting pressure. Eversion is much faster in the larger tunnel so the pulse is narrow even though the physical length of the larger and smaller tunnels are the same.

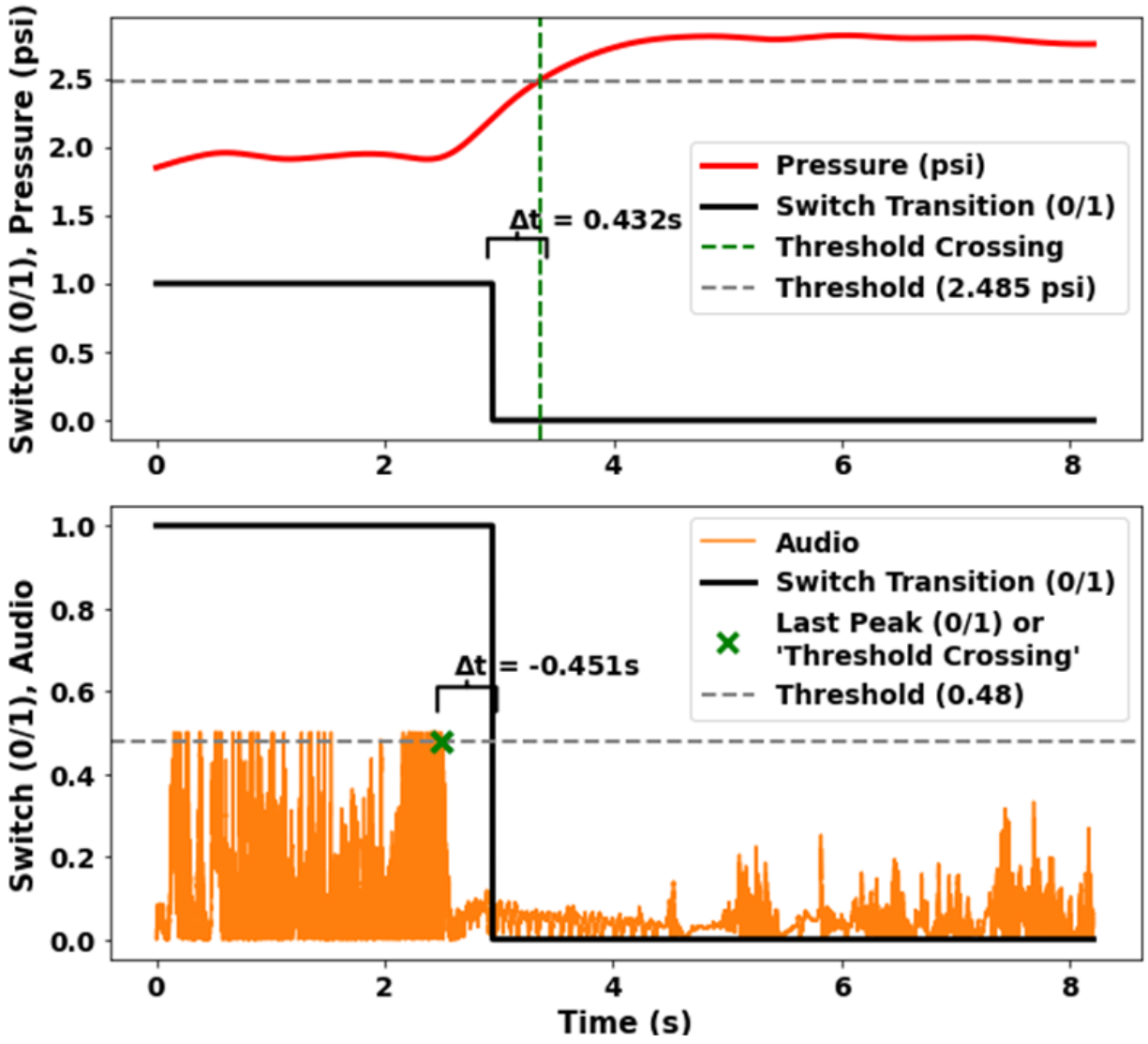

Figure 2.7: Pressure and audio signals from an LS transition. *Top*: Rectified and filtered pressure signal (red) crosses 2.485 psi threshold (dotted gray), and algorithm reports threshold crossing (green). Approximated tunnel transition by switch in (black). *Bottom*: Audio signal (orange) with peaks above 0.48 and last peak indicated by 'x'. Threshold crossing (green) is declared at the last peak. Approximated tunnel transition by switch in (black).

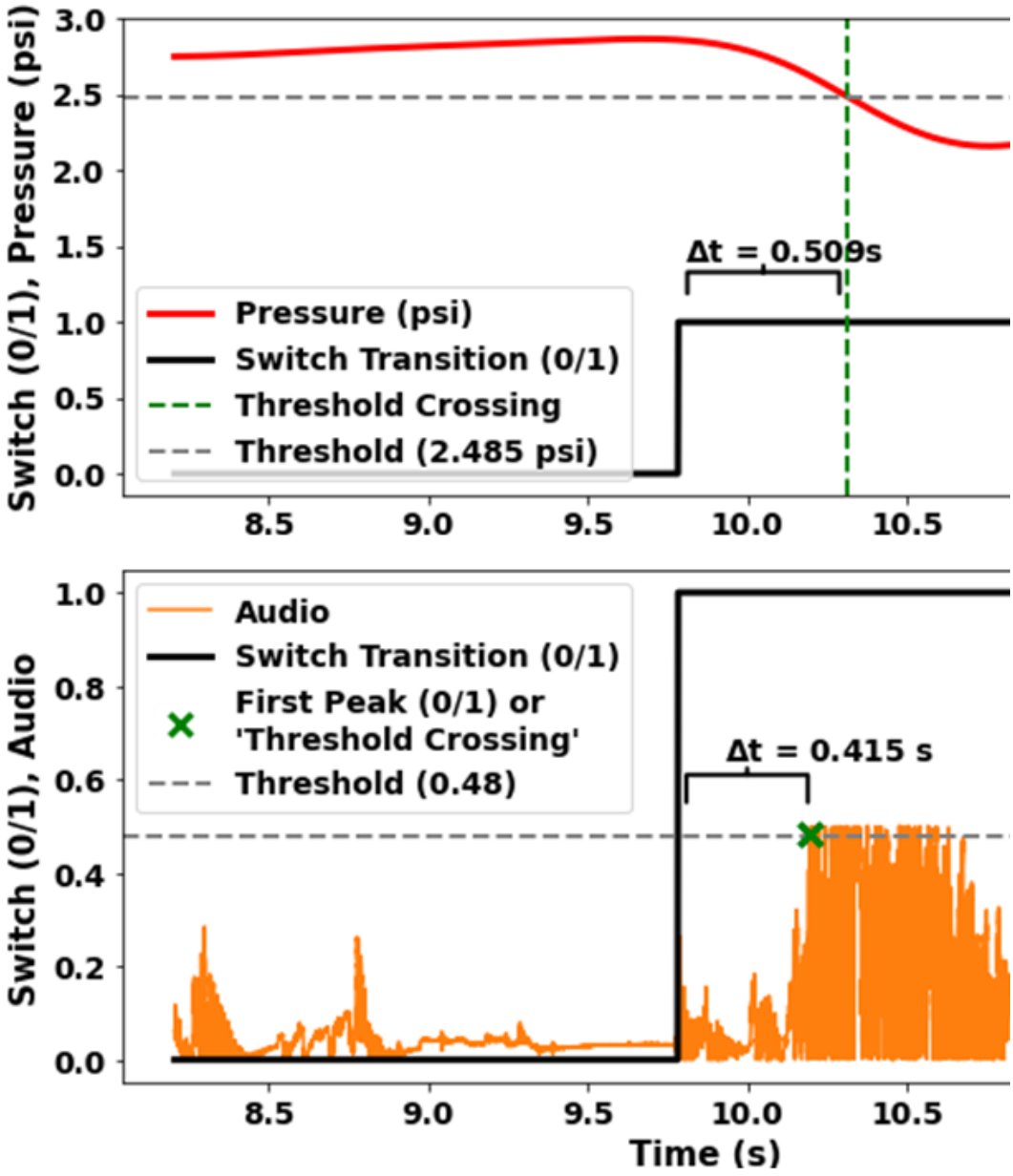

Figure 2.8: Pressure and audio signals from an SL transition. *Top*: Rectified and filtered pressure signal (red) crosses 2.485 psi threshold (dotted gray), and algorithm reports threshold crossing (green). Approximated tunnel transition by switch in (black). *Bottom*: Audio signal (orange) with peaks above 0.48 and first peak indicated by 'x'. Threshold crossing (green) is declared at the first peak. Approximated tunnel transition by switch in (black).

Figure 2.7 shows the results of the algorithms described in section 2.2.7 for an LS transition. The pressure thresholding algorithm is applied to the pressure signal (top). The threshold is 2.485 psi: the average of the upper limits (2.83 and 2.88 psi) and lower limits (2.06 and 2.17 psi). The time between the switch transition and pressure threshold crossing is 0.432 s. The audio thresholding algorithm is applied to the audio signal (bottom). The time between the audio peak's threshold crossing and switch transition is 0.451 s.

Figure 2.8 shows the results of the algorithms described in section 3.2.7 for an SL transition. The pressure thresholding algorithm is applied to the pressure signal (top). The thresholds are the same as 2.8. The time between the switch transition and pressure threshold crossing is 0.509 s. The audio thresholding algorithm is applied to the audio signal (bottom). The time between the switch transition and audio peak's threshold crossing is 0.415s.

The average time difference between threshold crossing and switch data was 0.162 s (standard deviation of 0.480 s) across all results (pressure and audio and all LS and SL transition results combined). Time differences from pressure and audio thresholding were combined by averaging. The average time delay based on pressure thresholding was 0.374 s (0.192 s) and, based on audio thresholding, was -0.050 s (0.578 s). The first transitions closer to the base of the vessel were LS1 and SL1 averaged -0.026 s (0.490 s). The second transitions further from the base of the vessel were LS2 and SL2 and averaged 0.350 s (0.388 s).

Table 2.1 displays time deltas from pressure and audio combined as well as distinct results from each. Pressure data has an overall smaller standard deviation (0.192 s) than the audio data (0.578 s), as made visible by the spread of the histograms in Figure 2.9. Table 2.1 also distinguishes time deltas from transitions located closer to the base of the vessel (proximal) and transitions further away, where the everting tube is longer (distal).

Using spectral analysis, ninety-five percent of the pressure signal's energy was calculated to lie below 140 Hz (Sec. 2.2.5). The FFTs show a greater decibel level and louder noise at lower frequencies (below $\sim$ 4 Hz, Fig 2.10). The spectrograms show blue horizontal bars

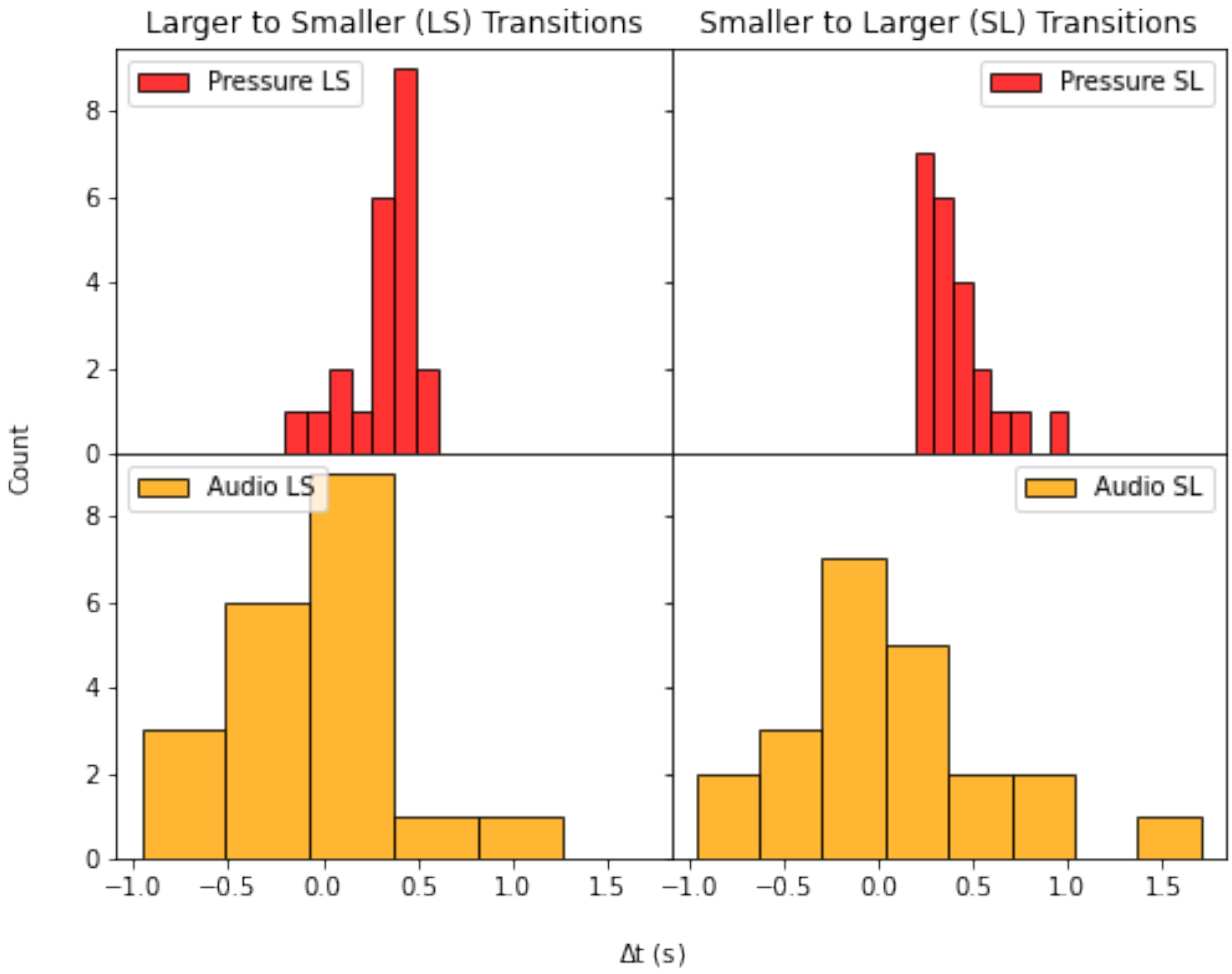

Figure 2.9: Time differences between switch transition and threshold crossing for 22 LS and 22 SL transitions. *Top*: Pressure (red). *Bottom*: Audio (orange). *Left-side*: LS transitions (n = 22). *Right-side*: SL transitions (n = 22).

Table 2.1: Time between threshold crossing and switch activation

Threshold Type	Mean (sec)	Std. Dev.
Audio and Pressure (A & P)	0.162	0.480
Pressure Alone	0.374	0.192
Audio Alone	-0.050	0.578
A & P (Proximal: LS1, SL1)	-0.026	0.490
A & P (Distal: LS2, SL2	0.350	0.388

aligning approximately with notches in the main FFT spectrum. The alignment is not exact because of different windowing lengths impacting time and frequency resolution.

Another spectral analysis was performed on isolated eversion sounds and also on an entire audio sample from the tunnel experiment using FFTs (Fig. 2.11 and 2.12) and spectrograms (Fig. 2.13). The FFTs are displayed by a zoomed in view from 140 Hz to 1 kHz in Fig. 2.11 and zoomed out view from 140 Hz to 12 kHz in Fig. 2.12). The isolated sounds are listed first and were studied first, before examining the larger audio sample. The FFT and spectrogram for *Switch Clicked* reflect a broadband sound. The spectrogram for *Friction of Reel* reflects a sound predominantly in the range 0-3 kHz, with a more distinct rise in decibel level at 3 kHz according to its FFT. The *Air Inflow* spectral results show a broader spectrum from 0-20 kHz which is loudest between 5 and 10 kHz. Finally, the spectral results for *Eversion into Tunnel* reflect intermittent, broadband sounds throughout the time duration.

The audio spectrogram of an entire tunnel experiment is shown in Figure 2.14. Each isolated sound described above is clearly distinguishable in the entire tunnel experiment recording including: (1) broadband sounds from *Eversion into Tunnel*; (2) broadband *Switch Clicked* sounds are identified; (3) *Air Inflow* which is loudest between 5 and 10 kHz; and (4) *Friction of Reel* the low-frequency energy band between 0 to 3 kHz.

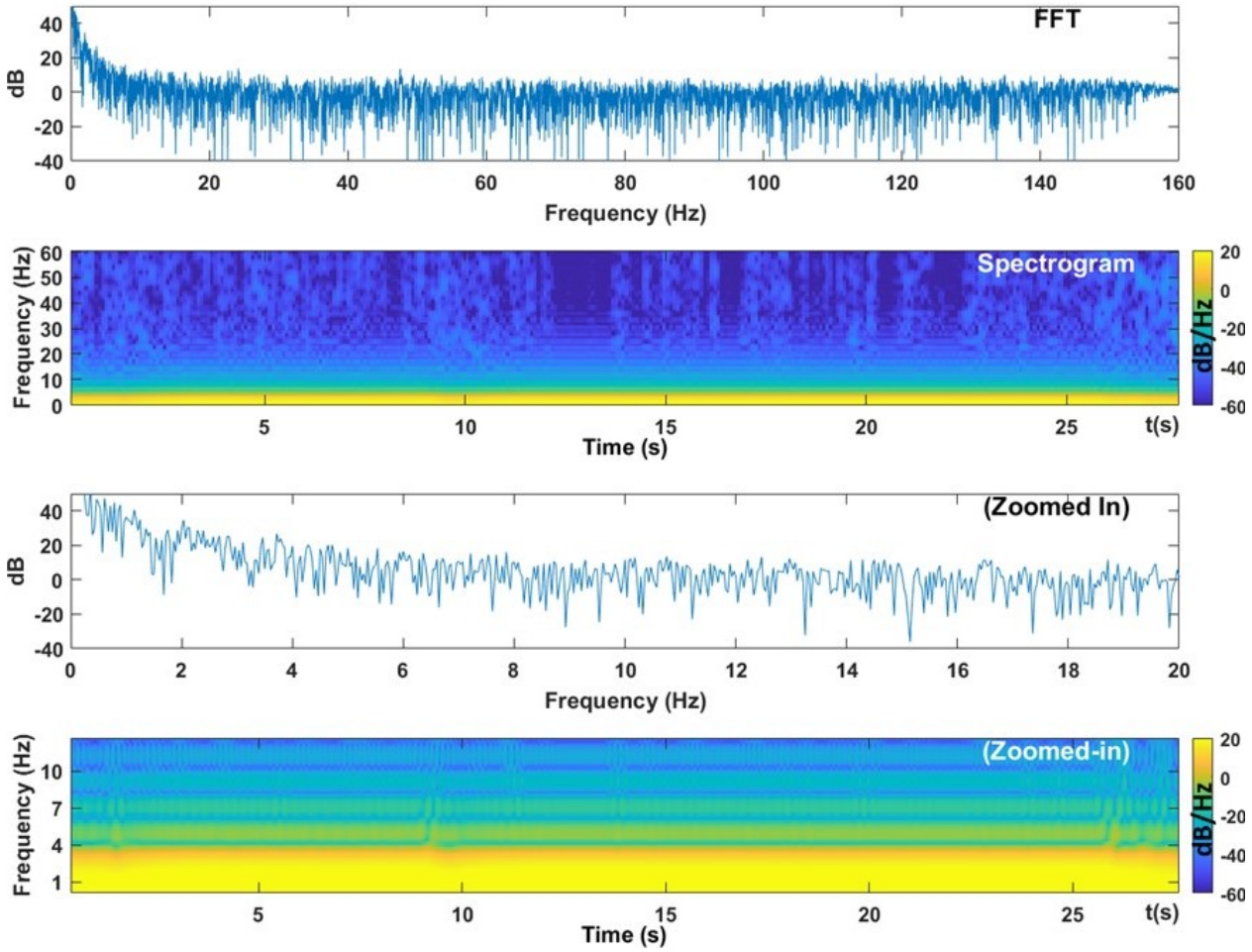

Figure 2.10: Pressure Frequency Analysis. FFT and spectrogram from a full tunnel test's pressure data.

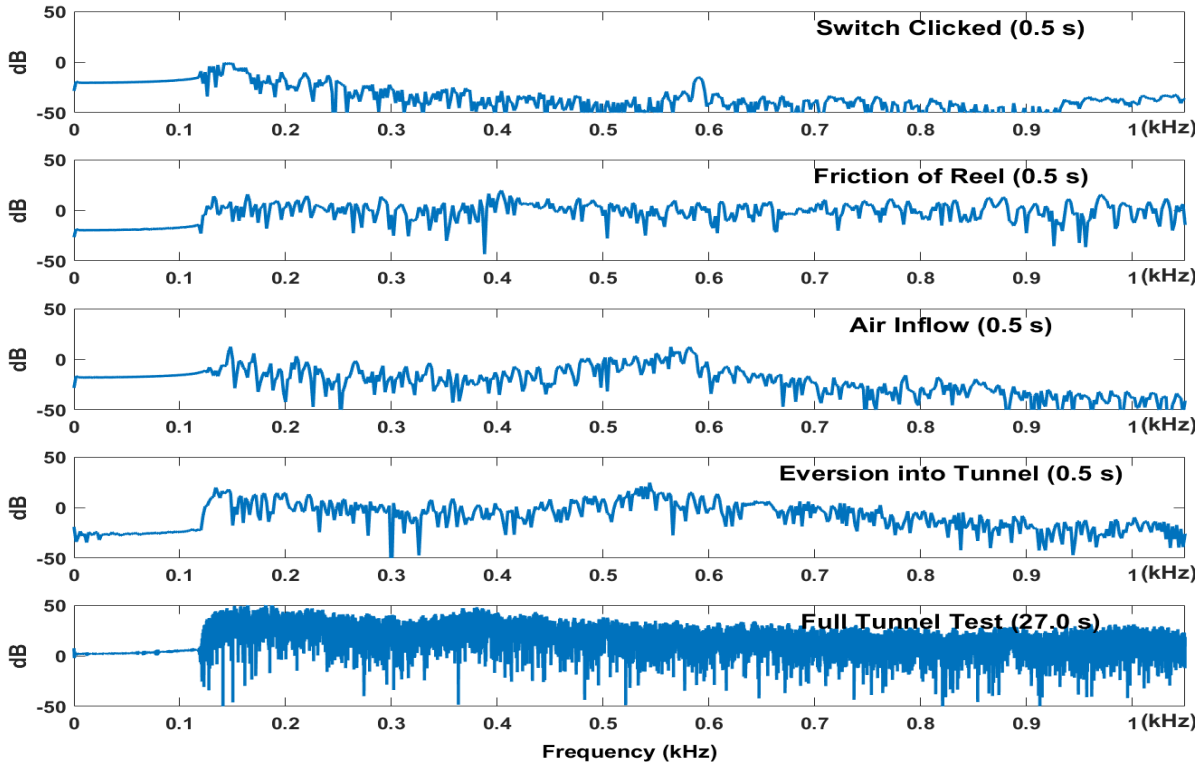

Figure 2.11: Audio FFTs of sound samples of isolated experiment components (0 to 1 kHz). Sounds are *Switch Clicked*, *Friction of Reel*, *Air Inflow*, *Eversion into Tunnel*, and a full tunnel test with all four transitions.

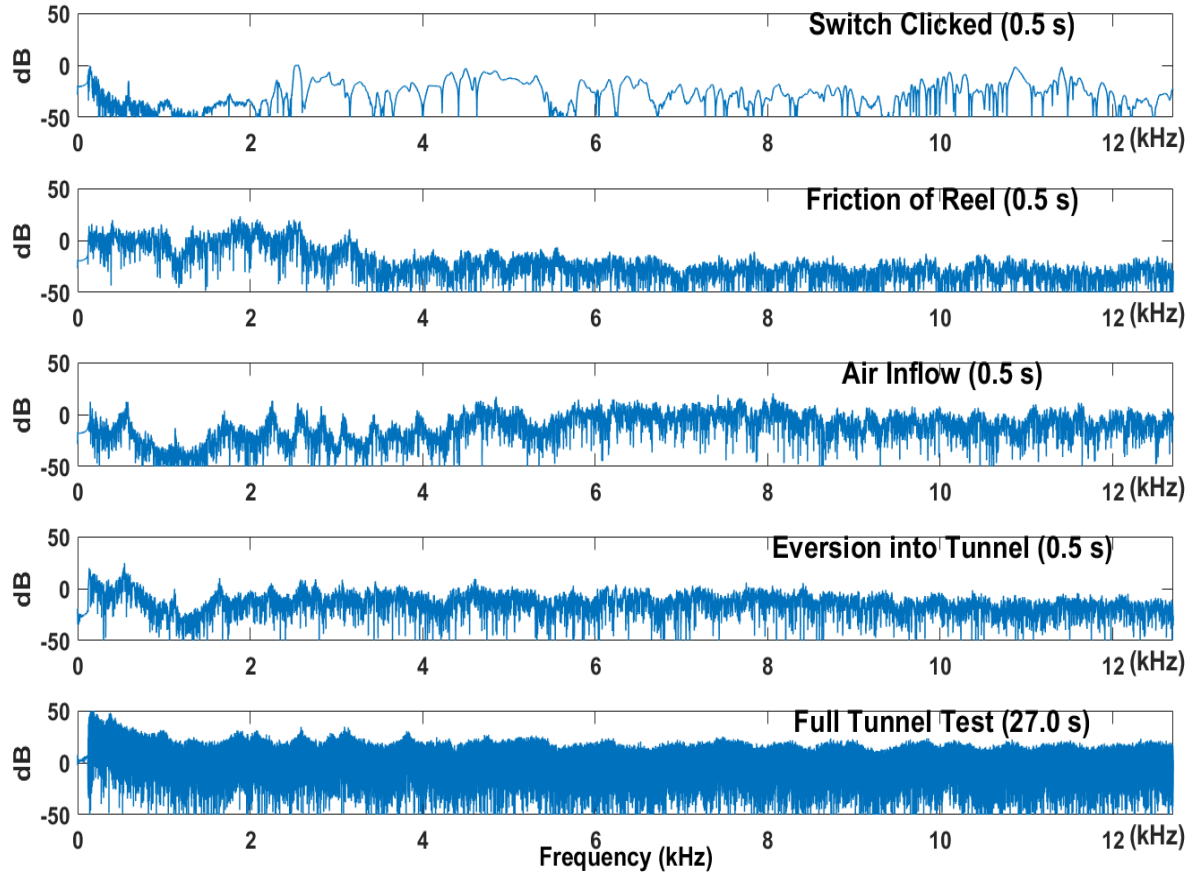

Figure 2.12: Audio FFTs of sound samples of isolated experiment components (0 to 12 kHz). Sounds are *Switch Clicked*, *Friction of Reel*, *Air Inflow*, *Eversion into Tunnel*, and a full tunnel test with all four transitions.

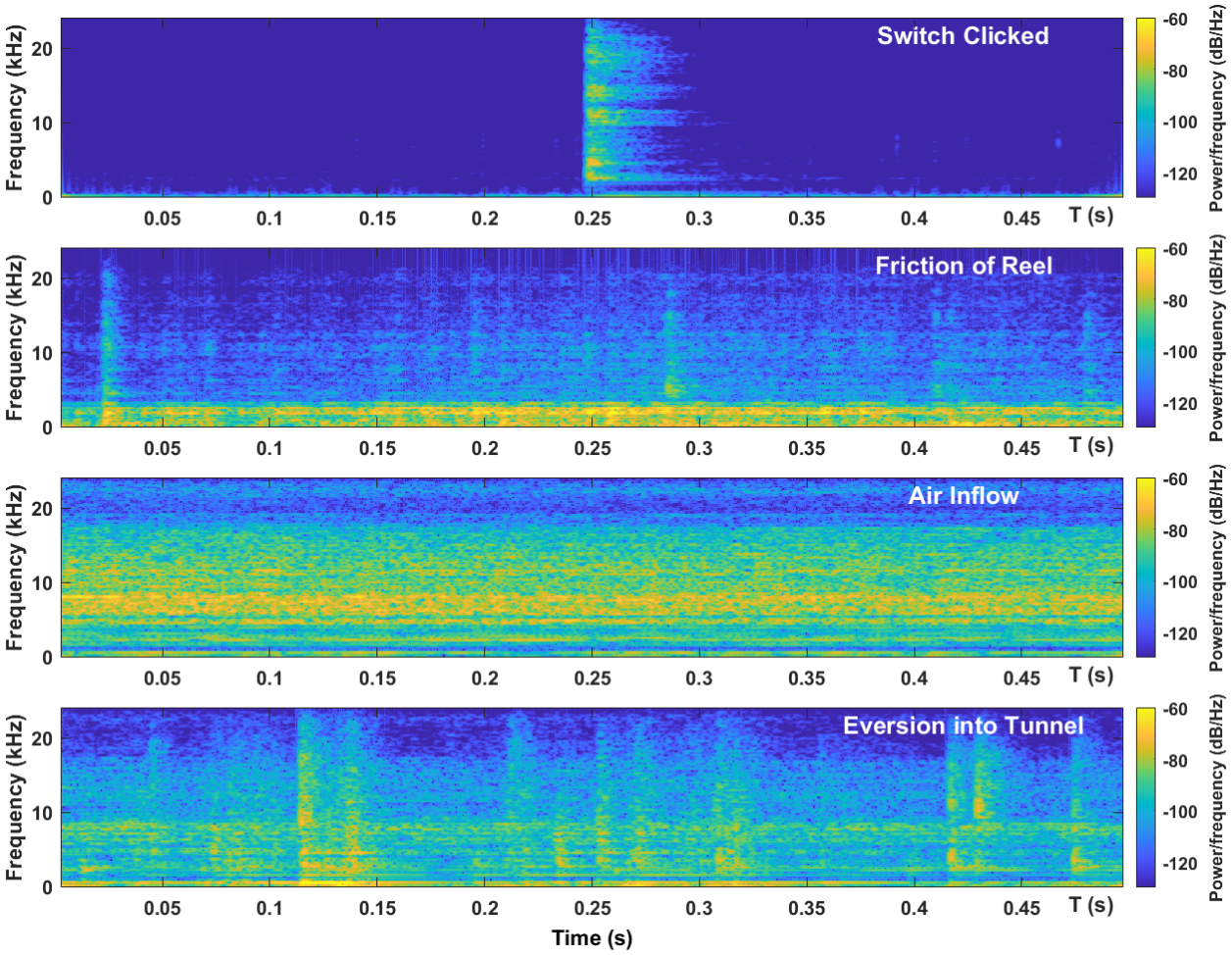

Figure 2.13: Audio spectrograms. Spectrograms from 0.5 s length sounds (top to bottom): *Switch Clicked*, *Friction of Reel*, *Air Inflow*, and *Eversion into Tunnel*.

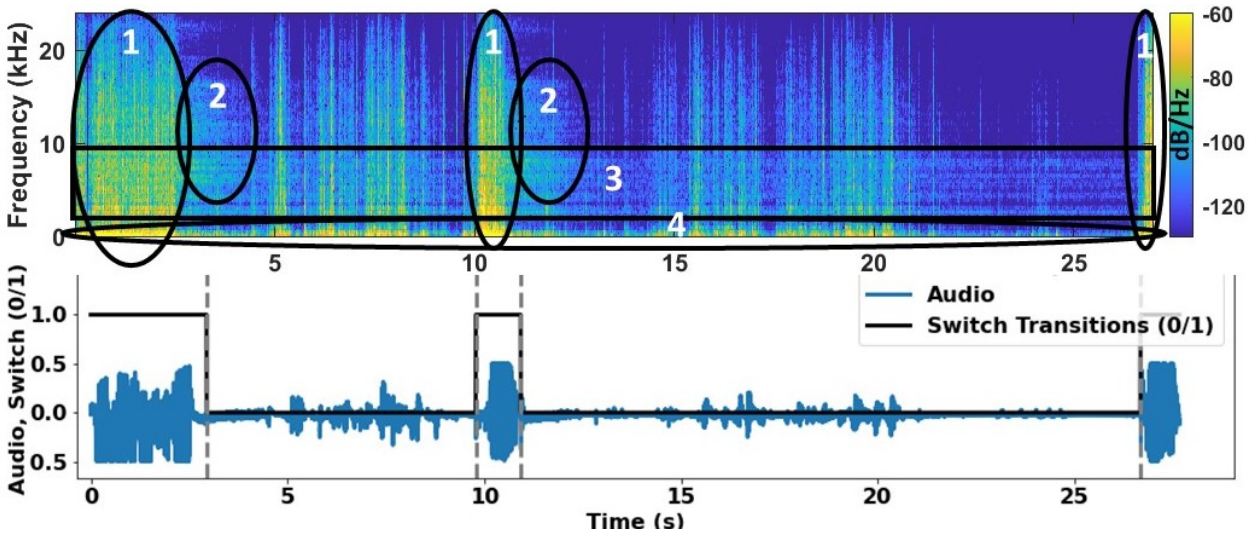

Figure 2.14: Top: Full tunnel test spectrogram. (1) Loud *Eversion into Tunnel*, (2) *Switch Clicked*, (3) *Air Inflow* and (4) *Friction of Reel*. Bottom: Audio and switch data.

2.4 Discussion

Acoustic signals indicate tunnel transitions of everting tubes. Pressure: In Figure 2.6, an everting tube in a larger tunnel requires less everting pressure, while in a smaller tunnel it requires more everting pressure, and it shows how this pressure rises and falls over time between tunnel transitions. For example, at the SL to LS transition at 9-11 s, the pressure dips at the smaller to larger transition and pressure immediately rises at the larger to smaller transition. Using thresholding at 2.485 psi, the pressure thresholding algorithm (Fig 2.7, top) identified this LS transition within 0.432 s. The pressure thresholding algorithm (Fig 2.8, top) identified the following SL transition within 0.509 s. One threshold was used across the entire signal, but to optimize detection in future studies, this 2.485 psi threshold can be separated into two values and shifted lower for an LS transition, and likewise, higher for an SL transition. Audio: In Figure 2.6, an everting tube in a larger tunnel generated louder sounds (faster speed), while in a smaller tunnel sounds are quieter (slower speed). For example, at the LS transition at ∼11 s, the audio immediately gets quieter. Using

thresholding at 0.48, the audio thresholding algorithm (Fig 2.7, bottom) identified this LS transition within 0.451 s. At the following SL transition, the audio thresholding algorithm (Fig 2.8, bottom) identified within 0.415 s.

Pressure and audio signal thresholding can estimate when tunnel transitions occur. We estimated transitions within 0.374 s (standard deviation of 0.192 s) using pressure signals, and -0.050 s (0.578 s) using audio signals. Results also indicate that length impacts acoustic sensing capabilities in everting tubes. The time to estimate a transition is proportional to the length of the tube. The time delays are longer for a longer everting tube, and shorter for a shorter everting tube with an average 0.114 s delay difference between the proximal and distal transition estimates. The everting tube grows at faster speeds proximal to the base of the vessel and grows at slowers speeds farther out and distally. Note the everting tube is shorter at one of the initial transitions (LS1 and SL2), and longer at one of the latter transitions (LS2 and SL2). Also note that time deltas are an approximate tool for evaluating sensing capabilities. A switch transition indicates an actual tunnel transition, $\pm$ 38.1 ms, and timing inaccuracies will vary in different set-ups at different everting speeds. Moreover, pressure thresholds were not optimized to reduce time delay.

Audio spectral analysis can classify sounds of everting tubes. Consider the FFTs (Figs. 2.11 and 2.12) and spectrograms (Fig 2.13) of the following isolated sounds. *Switched Clicked*: A click is a short, impulsive sound, and as expected, spectral plots show a broadband sound over a short time interval. The duration of the sound is likely prolonged by the echoing of the tube (see paragraph 4 of Sec. 5.1 for future studies for echoing). *Friction of Reel*: Since the material reel is mounted on ball bearings and the string is pulled at a constant speed, we expect and find a fairly constant sound. *Air Inflow*: Hissing sounds tend to be broader spectrum, and as expected, spectral plots show energy from 0-20 kHz that is loudest between 5 and 10 kHz. *Eversion into Tunnel*: The sounds of eversion should be broadband sounds because of crackling sounds from the LDPE plastic. They also should occur at irregular intervals because free eversion is nonlinear and irregular. Indeed, in the spectrogram, intermittent broadband sounds are shown at moments where the LDPE tubing exits the

tunnel and everts. You can also see the broader spectrum of airflow in the background of the spectrogram. Eversion sounds are better distinguished over time in the spectrogram, as this *Eversion into Tunnel* FFT generally looks like the *Air Inflow* FFT (Figs. 2.11 and 2.12).

Lastly, note that all the FFTs reflect 140 Hz LPFs and HPFs used to separate the audio and pressure signals, and that the Full Tunnel Test FFT (Figure 2.11 and 2.12) is densely detailed because it is has a longer duration and contains all the collected sounds in one sample.

These eversion sounds are clearly distinguished and labeled in the overall full constriction test's spectrogram (Fig. 2.14) and help indicate when tunnel transitions occur. A larger tunnel segment causes faster eversion and louder LDPE plastic crinkling and louder reel movement, thus (1) (as labeled in Fig. 2.14) sections have more prominent eversion sounds. When prominent eversion sounds (1) begin, an LS transition can be visually identified and when these broadband sounds cease, an SL transition can be visually identified. These LS and SL transitions line up with the switch transitions shown in the bottom of Fig. 2.14. Both (1) and (2) are broadband sounds, which would otherwise make them difficult to distinguish, but we know when switch clicking occurs from the limit switches. Around t = 3, a switch click is seen. There are two switch clicks back-to-back around t = 10 to 12 s, superimposed on eversion sounds and on one another. The remnants of the last switch click can be seen at about t = 12 s.

Chapter 3

CONSTRICTION EXPERIMENT

3.1 Introduction

In the previous experiment it was found that pressure and audio signals had distinguishable responses to tunnel transitions of everting tubes, and that these eversion sounds are distinguishable in audio spectrograms. However, we would also like to be able to identify if pressure and audio signals have different responses in differently sized tunnels. This experiment sends an everting tube through a significantly smaller tunnel or "constriction" and looks for differences in pressure and audio responses.

3.2 Methods

In this second experiment, an LDPE tube was freely everted into a long tunnel with a constriction while pressure and audio signals were captured (see glossary for "free eversion"). The previous experiment in Chapter 2 was designed to test if even a slight change in tunnel diameter was distinguishable in pressure and audio signal response. This experiment was designed with much more drastic changes to the tunnel size to test if pressure and audio signal responses would be more substantial and extreme. The smaller tunnel in this experiment was distinct from the smaller tunnels in the previous experiment because it was a shorter (1.27 cm vs 25.4 cm) in length and the opening had a significantly smaller cross-sectional area ratio (2.25 vs 6.25 to the larger tunnel). Based on its shorter and tighter dimensions (1.27 cm length x 1.27 cm diameter), it is more aptly named a "constriction" rather than a "smaller tunnel". The cross-sectional area of larger tunnels remained the same.

A total of 20 samples were collected (2 transitions per trial x 10 trials = 10 entering constriction transitions (TR1) and 10 exiting constriction transitions (TR2)).

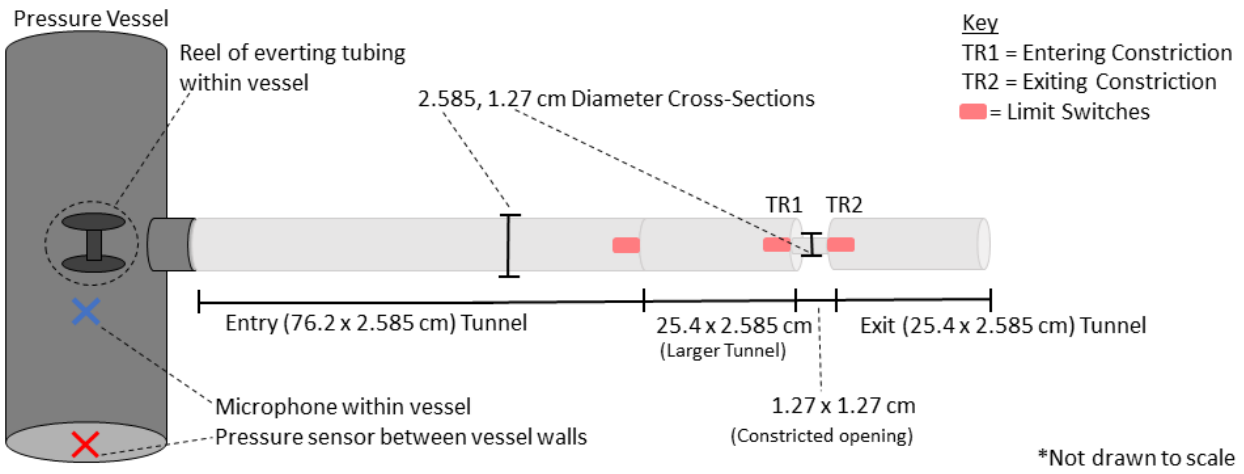

Figure 3.1: Experimental Setup (Constriction Experiment). Opening of pressure vessel sends everting tube directly into tunnels.

3.2.1 Soft Everting Robot

Like the first experiment (Sec.2.2.1), LDPE tubing with 3.81 cm flat width and 2mil (0.05mm) wall thickness was used as the everting material. The tubing takes on a 2.858 cm diameter, and maintains that same diameter, when fully inflated from 3 to 8 PSI.

3.2.2 Tunnel and Switches

An everting tube was grown into a multi-section tunnel composed of PVC and copper pipe (Fig. 3.1, 3.3). The experiment tunnel begins with an entry tunnel (76.2 cm long with a 2.858 cm internal diameter (76.2 cm x 2.858 cm)), which gives space for growth of the free everting tube to stabilize and for pressure to build up to the standard everting pressure of the larger tunnel (∼2 psi). The entry tunnel was followed by 3 alternating-sized (length x internal diameter) sections: an identical PVC section 25.4 cm x 2.858 cm, a small constriction 1.27 cm x 1.27 cm, and another identical diameter section 25.4 cm x 2.858 cm. The constriction is built from a copper (1.27 cm x 1.27 cm) pipe and connected to the PVC section with foam (Fig. 3.4). Limit switch arms were carefully positioned at the end of each alternating section.

The first switch was used as a locational reference point and detected entry into the first 25.4 cm x 2.858 cm section. The remaining two switches detected the notable transitions: when the tube was entering the constriction (TR1) and exiting the constriction (TR2).

Limit switches were positioned such that passage through the diameter transition events was detected within ± 38.1 ms accuracy (Section 2.2.1). This limit switch accuracy is applicable to this experiment as a worst case scenario because this accuracy may only increase to due to increased everting tube speeds. The increased flow from the air supply produced a faster speed than the previous experiment, as seen by comparing Figure 3.2 vs 2.3. Additionally, the last switch that recorded the constriction exit (TR2) would have an even better accuracy because the everting tube exited the constriction at a very high speed as seen in Figure 3.6 (a phenomenon discussed later in this paper). But, for the sake of consistency, a ± 38.1 ms accuracy can be assumed across all limit switches. Each switch was positioned at the end of a tunnel segment to detect a transition, except in this experiment the last switch was positioned at the start of a tunnel segment. The constriction segment was too small for a switch. To detect this transition, the switch was placed at the start of the next tunnel segment (Fig. 3.5). This positioning and orientation ensured sensitivity and accuracy of the switch.

3.2.3 Air Supply

Like the experiment in Chapter 2, a 10 lb air tank was connected to a proportional controlled pressure regulator (SMC Electro-Pneumatic (E/P) regulator ITV2011-04N2N4) to supply very stable input pressure to a needle valve that was locked in position to create a steady flow into the pressure vessel at the everting tube base. This flow was set at 1130 cm^3/s (greater than the 900 cm^3/s flow rate from the previous experiment). The flow rate was estimated from a video of an everting tube growing alongside an imperial ruler (converted to metric) (Fig 3.2). Using two reference points for pressure (P) and volume(V), the difference in cylindrical volume was found and Boyle's law was applied, $P_1V_1 = P_2V_2$.

The flow rate was manually set using the E/P regulator and needle valve. Both the

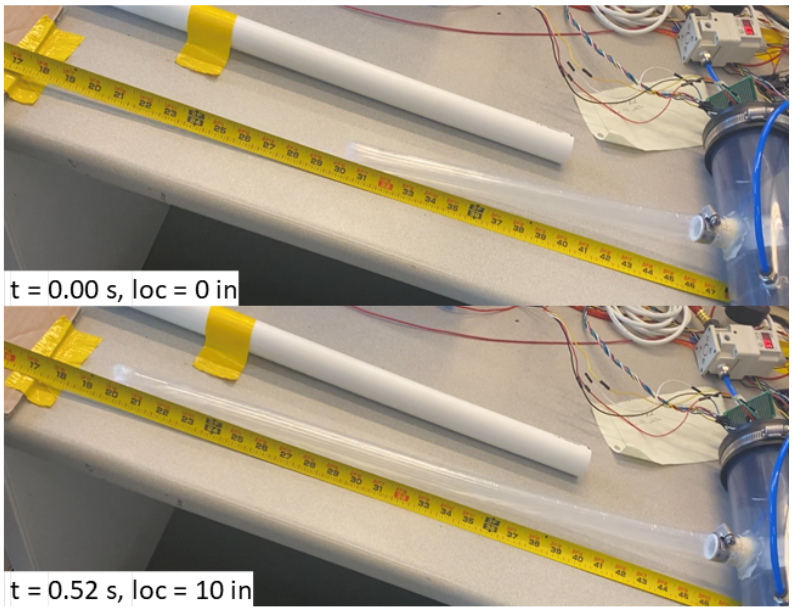

Figure 3.2: Flow Rate Video Frame Analysis. Video frames spanning 0.52 s and 25.4 cm used in flow rate calculations.

pressure of the E/P regulator and the resulting flow rate were raised until the everting tube could pass the constriction. The constriction required a higher everting pressure than the tunnels in the previous experiment. A higher supply pressure from the E/P regulator was required to achieved a higher flow rate (230 cm^3 higher as in Sec. 2.2.3). Supply pressure must be greater than the everting pressure in the constriction, which was ~6-8 psi.

3.2.4 Sensors

As in Chapter 2, a pair of sensors in the pressure vessel collected a full spectrum of pressure signals, accurate from 0 to 10 kHz. See Section 2.2.4 for details.

3.2.5 Filtering and Windowing

Audio (microphone sensor data) was Hamming windowed to help reduce DC component spikes at 0 Hz and high-pass filtered to remove frequencies detected by the pressure sensor.

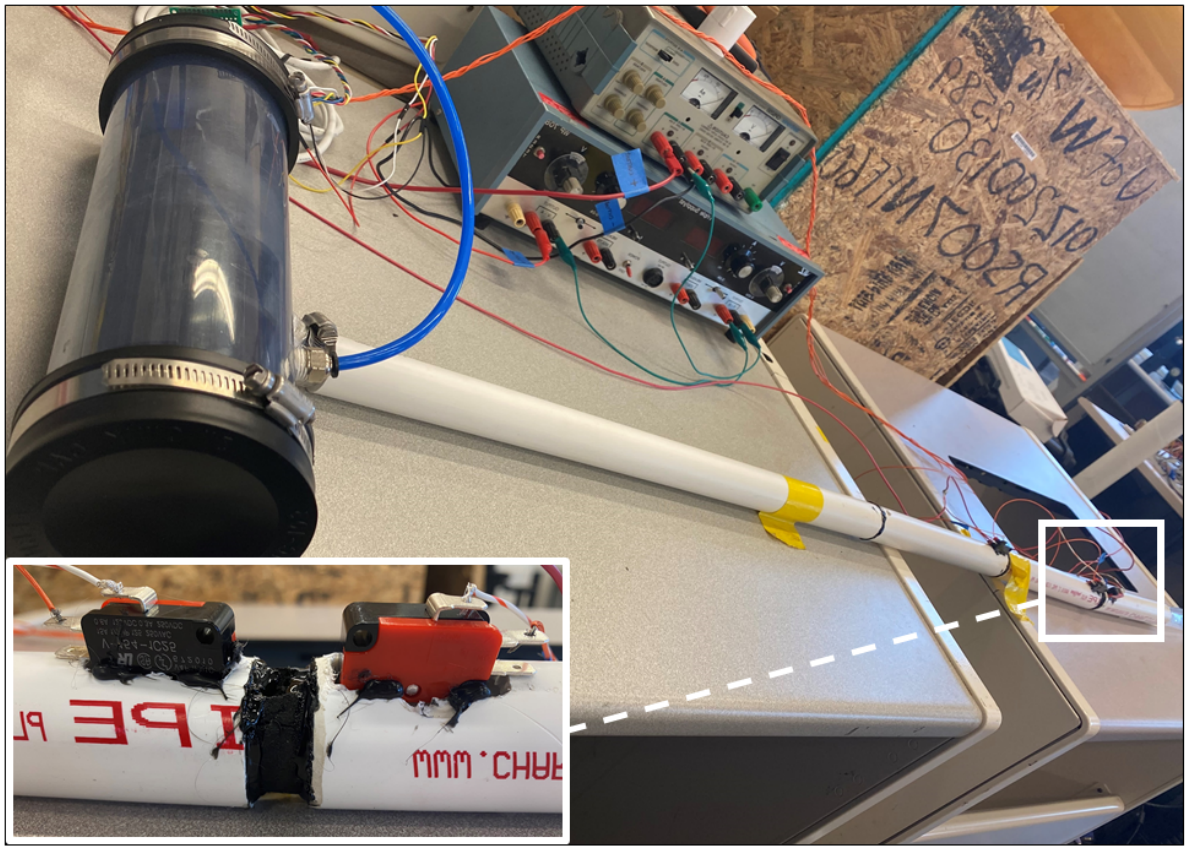

Figure 3.3: Desktop Setup (Constriction Experiment). *Main Image*: Pressure vessel, tunnels, power supplies. *Bottom right*: Close up of the constriction and switches.

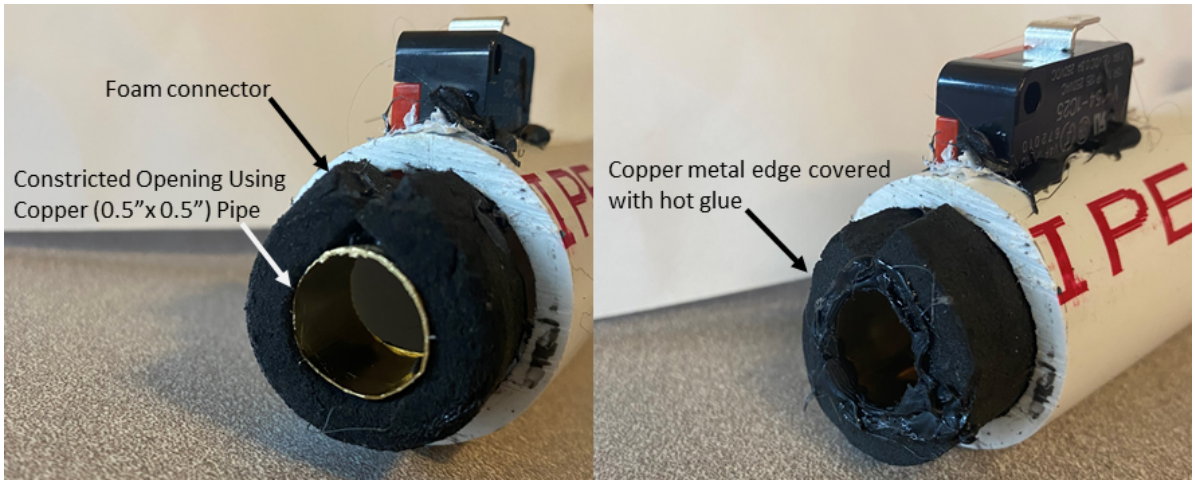

Figure 3.4: Constriction build. *Left*: Copper (1.27 cmx1.27 cm) pipe forms constricted opening. Foam connects to PVC pipe. *Right*: Copper metal edge covered with black hot glue to prevent puncture to everting tube.

As in the experiment in Chapter 2, a 140 Hz low-pass filter (LPF) was applied on the pressure data, and a 140 Hz high-pass filter (HPF) was applied on the audio data as in the experiment. The same filter was applied to maintain consistency and still ensured accurate, full spectrum collection based on the following considerations: 1) 140 Hz LPF cutoff is almost a factor of 5 below the pressure sensor's sampling rate, and 2) 95% of the pressure signal's energy was calculated to lie below 190 Hz, which is close to the 140 Hz result from the previous experiment (2.2.5). 3) In the microphone's datasheet, the frequency response performance curve starts to roll off below 100-200 Hz and above 10 kHz. The 95% window of audio energy was calculated to lie below 8155 Hz, negligibly different from the previous experiment, 8341 Hz (2.2.5). Since the microphone's performance curve does not begin to roll off until 10 kHz, we know we accurately sampled the full spectrum.

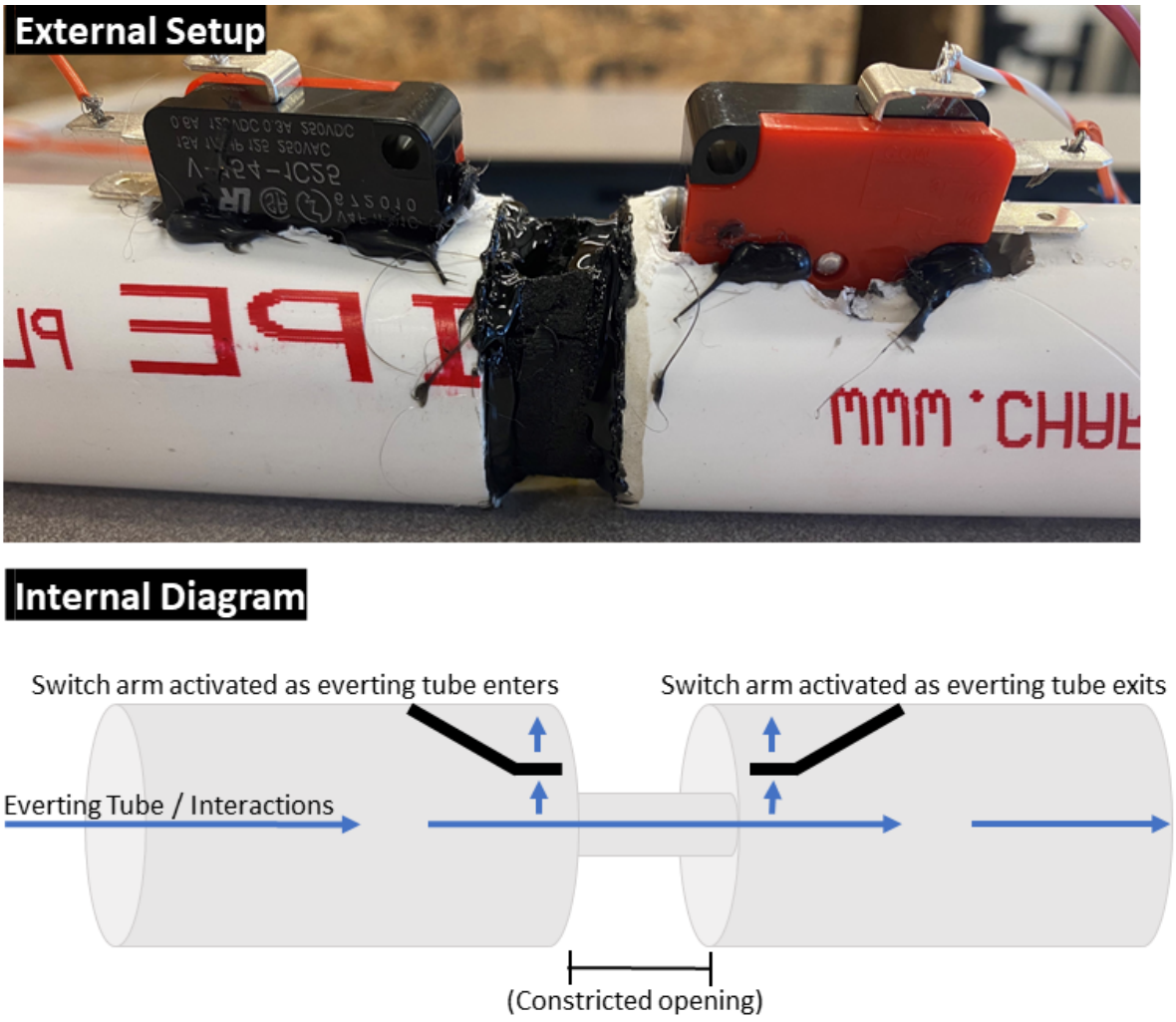

Figure 3.5: Switch placement detecting constriction entry / exit. *External Setup*: Orientation reversed for the leftmost (last) switch. *Internal Diagram*: Everting tube travels right to left. Switch arms (black) activated as everting tube enters and exits constricted opening.

3.2.6 Sound Classification

Isolated eversion sounds from the experiment in Chapter 2 (Section 2.2.6) were used to distinguish sounds in the samples' spectrograms (*Switch Clicked*, *Friction of Reel*, *Air Inflow* and *Eversion into Tunnel*).

3.2.7 Thresholding Algorithms

We programmed two post-processed thresholding algorithms for pressure and audio time domain signals. These algorithms complete the same task as in 2.2.7, but the pressure algorithm's method for calculating the threshold was slightly modified to analyze one transition at a time. It applied a Butterworth filter to the pressure signal and found the initial moment it crossed a threshold. This same threshold was used for the entire signal, computed by an average of pressure samples from two tunnels (constituting an upper limit and lower limit pressure). The upper limit was the maximum pressure in the constriction. The lower limit was the minimum everting pressure in the initial larger tunnels (once the pressure was stabilized in part of the entry tunnel and first 25.4 cm x 2.858 cm section). As in 2.2.7, the audio thresholding algorithm analyzed one transition at a time. It took the magnitude of the signal and detected transient peaks above a threshold. In the TR1 transition, the algorithm found the last peak and declared a threshold crossing. Similarly, in the TR2 transition, the algorithm found the first peak and declared a threshold crossing. Across all samples, the threshold could have been placed lower than 0.48 to further minimize time delays between the switch transition and the threshold crossing. But, to stay consistent with the first experiment in 2 the audio threshold was kept at 0.48.

While in the constriction, pressure built to ∼7-8 PSI. Due to this high pressure, when exiting the constriction and entering the last (25.4 cmx2.858 cm) section, the everting tube grew very fast. A video frame analysis of this exit was performed as shown in Fig 3.6). From the frames, we know it was inside the last tunnel section for $\sim$ 0.07 s. It then exited the tunnel and traveled an additional 25.4 cm outside the tunnel over 0.08 s. The total

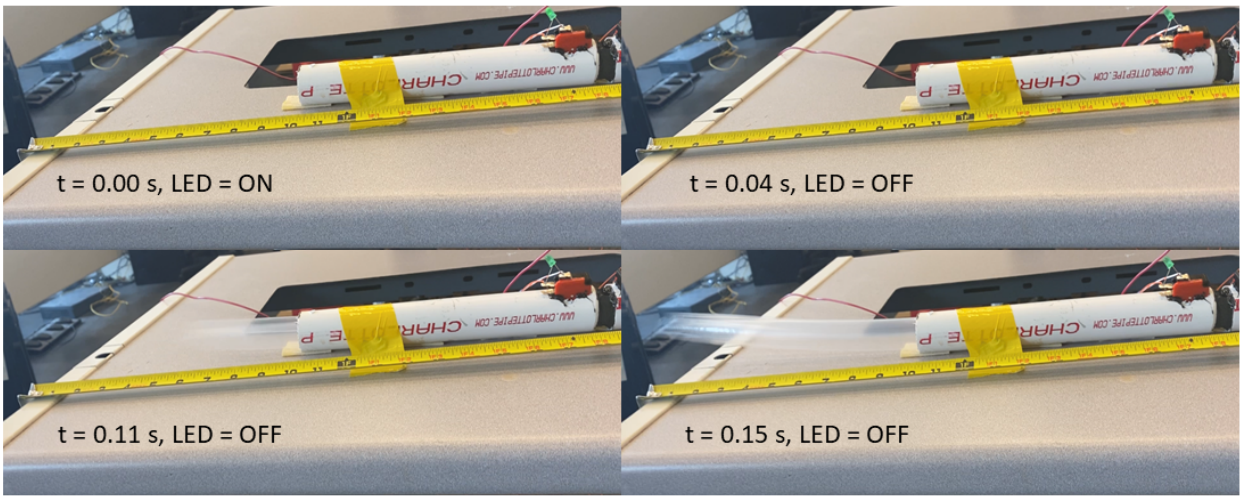

Figure 3.6: Exit Video Frame Analysis. t = 0 : last video frame LED is fully on (LED turns off between t = 0 and t = 1). t = 1 : first video frame LED is fully off. t = 2 : first video frame everting tube is visible outside tunnel. t = 3 : everting tube travelled $\sim$ 25.4 cm from end of tunnel. Exact times for t = 0, 1, 2 and 3 are t = 0.00, 0.04, 0.11 and 0.15 s.

time spanned was 0.15 s. When trimming the end of the signal, it must not be clipped before a signal response occurs. There may be a delay before the signal response reflect a transition and the algorithms need to be given ample time to detect a crossing from the signal response. Therefore, data signals were trimmed 0.15 s after TR2 (the transition exiting the constriction). Even though the everting tube was outside the tunnels at this point, the time lapse between the 25.4 cm tunnel section and the 25.4 cm free air section only differed by 0.01 s as it was traveling at approximately the same speed, and it is unlikely that this affected our pressure or audio data much. If this experiment were repeated, a longer 50.8 cm end tunnel section should be used.

3.2.8 Signal Trimming

Signals were trimmed or "cropped" to cover events of interest using the same method as the previous experiment (Sec. 2.2.8).

3.2.9 Spectrograms

Spectrograms and FFTs were generated from time domain signals and trimmed using the same method as the previous experiment in Sec. 2.2.9.

3.3 Results

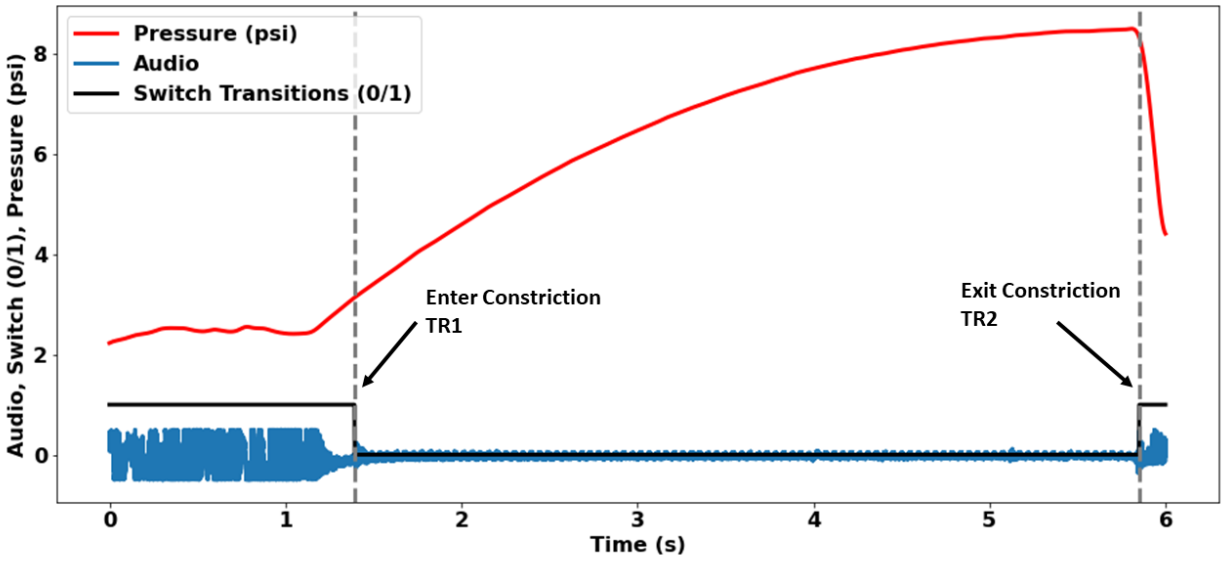

Figure 3.7: Pressure and audio transients. *Top*: Pressure signal (red, butterworth filtered) holds 2 psi in main larger tunnel, and rises to 8 psi in constriction, and falls after exit. *Bottom*: Audio signal (blue) overlaid with limit switch data (black) approximating tunnel transitions.

A sample growth trial will be discussed throughout the results section and in Figures showing single trial data (3.7, 3.8, 3.9 and 3.11). However, the results hold for all other trials.

In this sample trial, everting pressure is ∼2 psi in the main larger tunnel and rises to about ∼8 psi in the constriction (Fig 3.7). The audio is around 0.5 <unitless> peak-to-peak

in the main larger tunnel and 0.1 peak-to-peak in the constriction. The limit switch signal (black) indicates tubing diameter (1 = large, 0 = small). The first transition (TR1) is when the everting tube enters the constriction from the main larger tunnel. The second transition (TR2) is when the everting tube exits the constriction into the main larger tunnel. In TR1 (1→0), pressure rises over time to the everting pressure needed to pass the constriction. In TR2 (0→1), pressure drops (∼3→2 psi) from the constriction's everting pressure to the main larger tunnel's everting pressure.

Figure 3.8 shows the results of the algorithms described in section 3.2.7 for TR1. The pressure thresholding algorithm is applied to the pressure signal (top). The threshold is 5.36 psi: the average of the upper limit (8.49 psi) and lower limit (2.23 psi). The time between the switch transition and pressure threshold crossing is 0.986 s. The audio thresholding algorithm is applied to the audio signal (bottom). The time between the audio peak's threshold crossing and switch transition is 0.212 s.

Figure 3.9 shows the results of the algorithms described in section 3.2.7 for TR2. The pressure thresholding algorithm is applied to the pressure signal (top). The thresholds are the same as 3.8. The time between the switch transition and pressure threshold crossing is 0.108 s. The audio thresholding algorithm is applied to the audio signal (bottom). The time between the audio peak's threshold crossing and switch transition is 0.002 s.

The average time difference between threshold crossing and switch data was 0.070 s (standard deviation of 0.406 s) across all results (pressure and audio and all TR1 and TR2 transition results combined). The average time delay based on pressure thresholding was 0.347 s (0.321 s) and, based on audio thresholding, was -0.207 s (0.269 s). The first transition (TR1), where the everting tube entered the constriction, averaged 0.077 s (0.568 s). The second transition (TR2), where the everting tube exited the constriction, averaged 0.063 s (0.078 s).

Table 3.3 displays time deltas from pressure and audio combined as well as distinct results from each. Pressure data has positive time delay (mean 0.347 s) while the audio data has a negative time delay (-0.207 s), as made visible by the skew of the histograms in Figure 3.10.

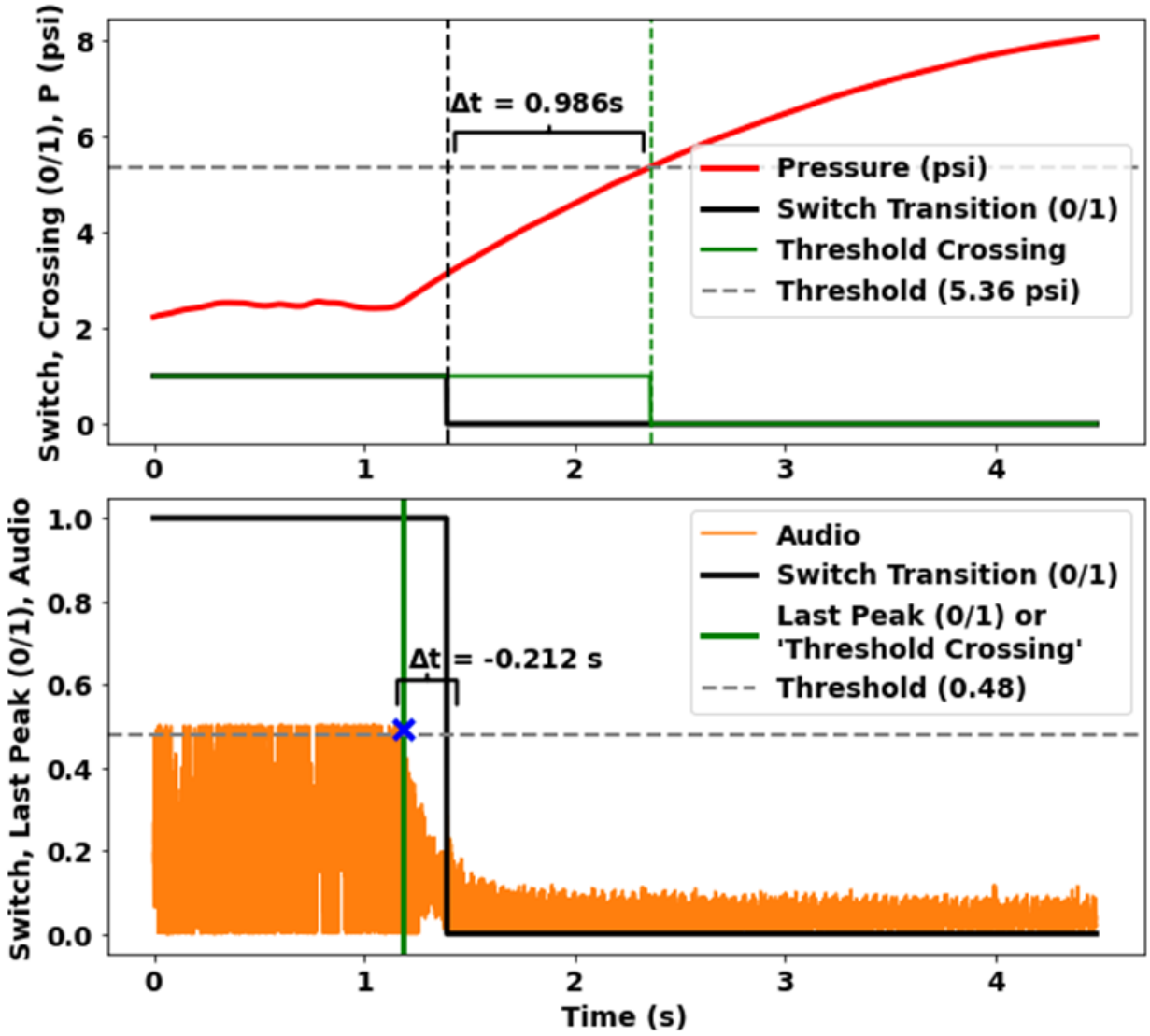

Figure 3.8: Pressure and audio signals from entry into constriction (TR1). *Top*: Rectified and filtered pressure signal (red) crosses 5.39 psi threshold (dotted gray), and algorithm reports threshold crossing (green). Approximated tunnel transition by switch in (black). *Bottom*: Audio signal (orange) with peaks above 0.48 and last peak indicated by 'x'. Threshold crossing (green) is declared at the last peak. Approximated tunnel transition by switch (black).

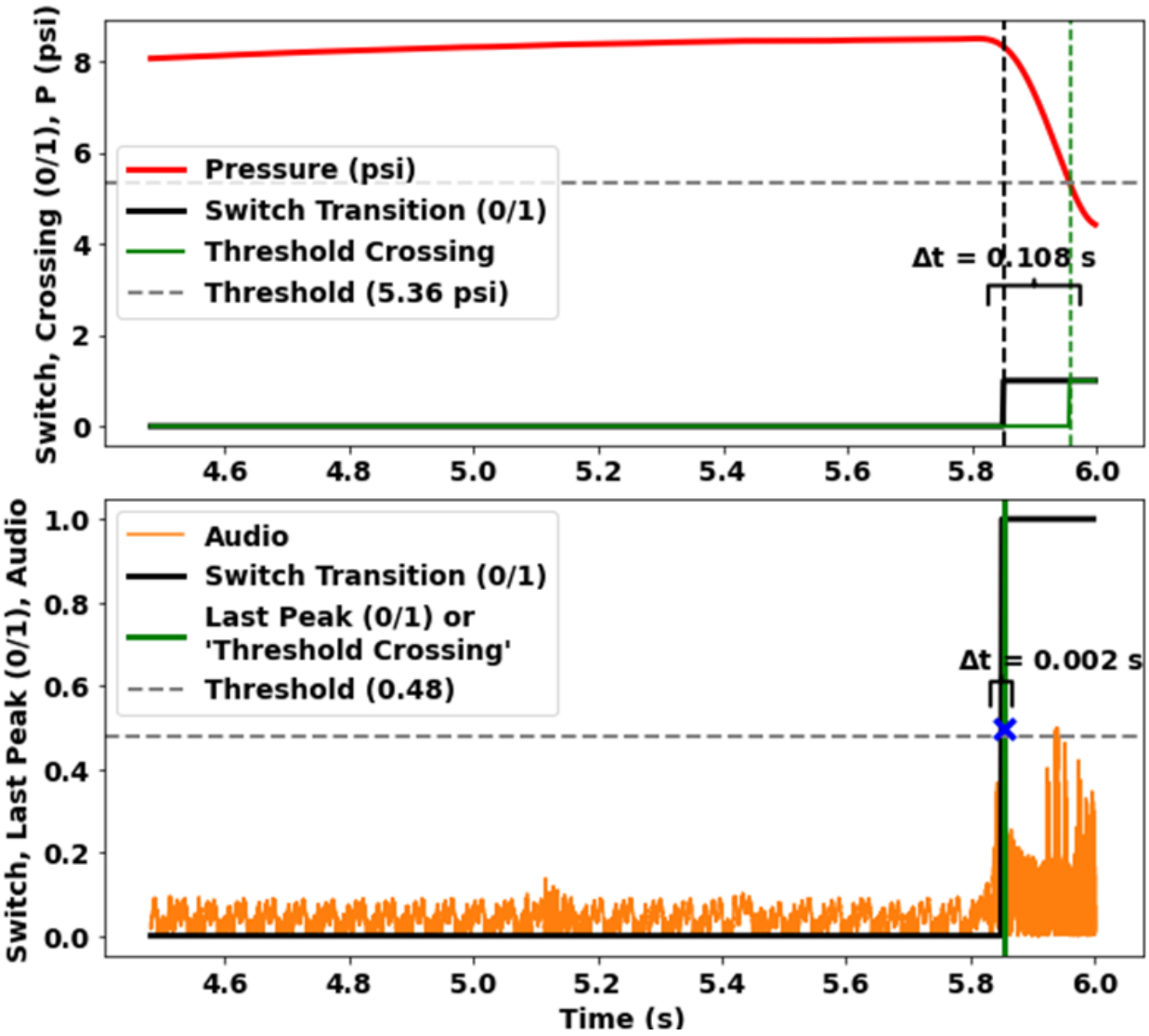

Figure 3.9: Pressure and audio signals from exit from constriction (TR2). *Top*: Rectified and filtered pressure signal (red) crosses 5.36 psi threshold (dotted gray), and algorithm reports threshold crossing (green). Approximated tunnel transition by switch in (black). *Bottom*: Audio signal (orange) with peaks above 0.48 and first peak indicated by 'x'. Threshold crossing (green) is declared at the first peak. Approximated tunnel transition by switch (black).

Table 3.1: Time between threshold crossing and switch activation

Threshold Type	Mean (sec)	Std. Dev.
Audio and Pressure (A & P)	0.070	0.406
Pressure Alone	0.347	0.321
Audio Alone	-0.207	0.269
A & P (TR1)	0.077	0.568
A & P (TR2)	0.063	0.078

Table 3.3 also distinguishes time deltas from entering and exiting transitions (TR1 vs TR2).

Using spectral analysis, ninety-five percent of the pressure signal's energy was calculated to lie below 140 Hz (Sec. 3.2.5). The FFTs show a greater decibel level and louder noise at lower frequencies (below $\sim$ 4 Hz in Fig 3.11). The spectrograms show blue horizontal bars aligning approximately with notches in the main FFT spectrum. The alignment is not exact because of different windowing lengths impacting time and frequency resolution. An increase in decibel level and loudness can be observed at t = 6 s when the everting tube very quickly and loudly exited the constriction.

Isolated sounds from experiment 1 (Fig. 2.13) are used to identify eversions in the audio spectrogram of an entire sample, shown in Figure 3.12. Each isolated sound described above is distinguishable in the entire sample's recording including: (1) broadband sounds from *Eversion into Tunnel*; (2) broadband *Switch Clicked* sounds are identified; (3) *Air Inflow* which is loudest between 5 and 10 kHz; and (4) *Friction of Reel* the low-frequency energy band between 0 to 3 kHz.

3.4 Discussion

This experiment reconfirms that pressure and acoustic signals indicate tunnel transitions of everting tubes (differences between experimental results discussed in Chapter 4). Pressure: In Figure 3.7, the everting tube in the larger tunnels requires less everting pressure, while in

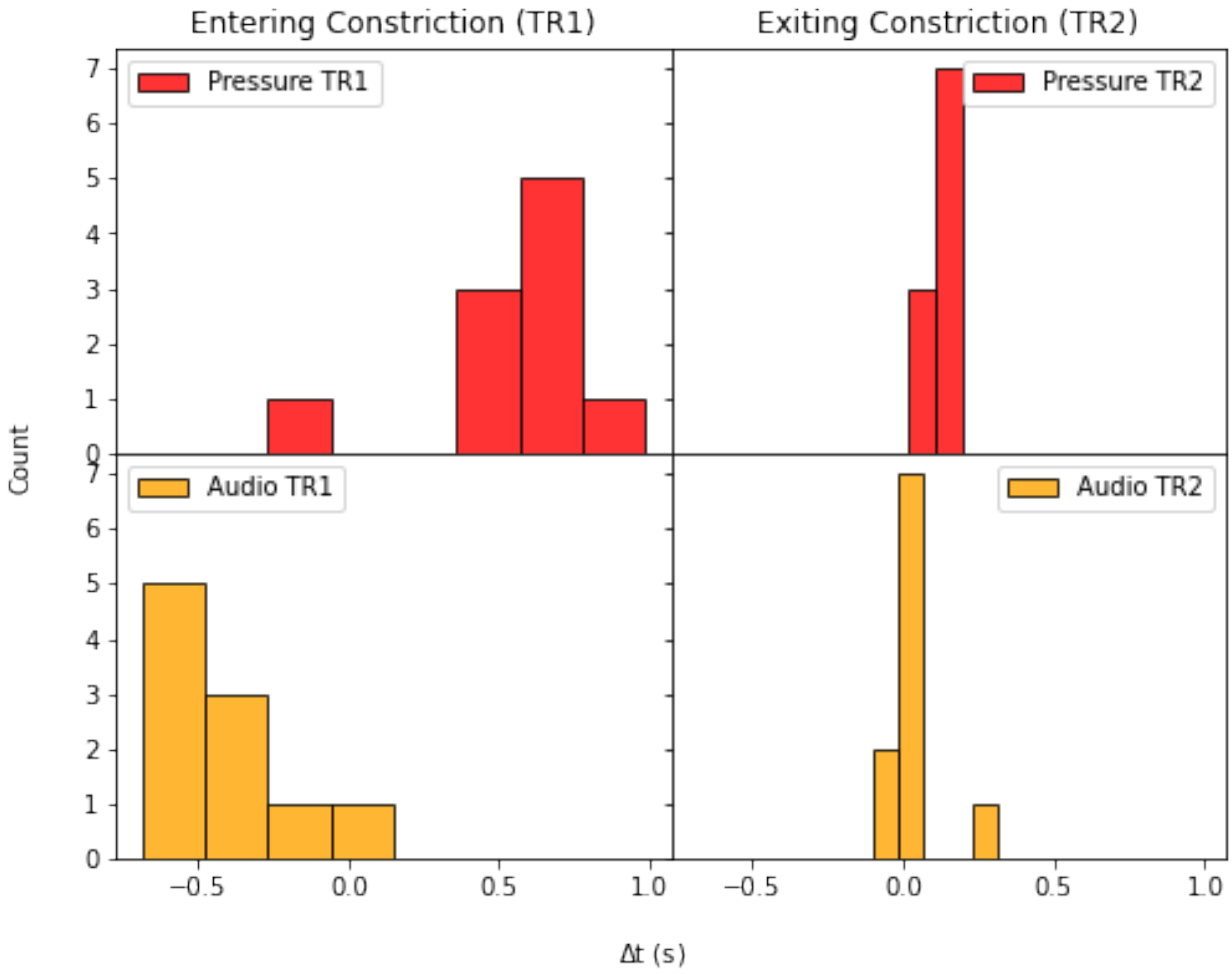

Figure 3.10: Time differences between switch transition and threshold crossing for 10 TR1 and 10 TR2 transitions. *Top*: Pressure (red). *Bottom*: Audio (orange). *Left-side*: Entering constriction (TR1, n = 10). *Right-side*: Exiting constriction (TR2, n = 10).

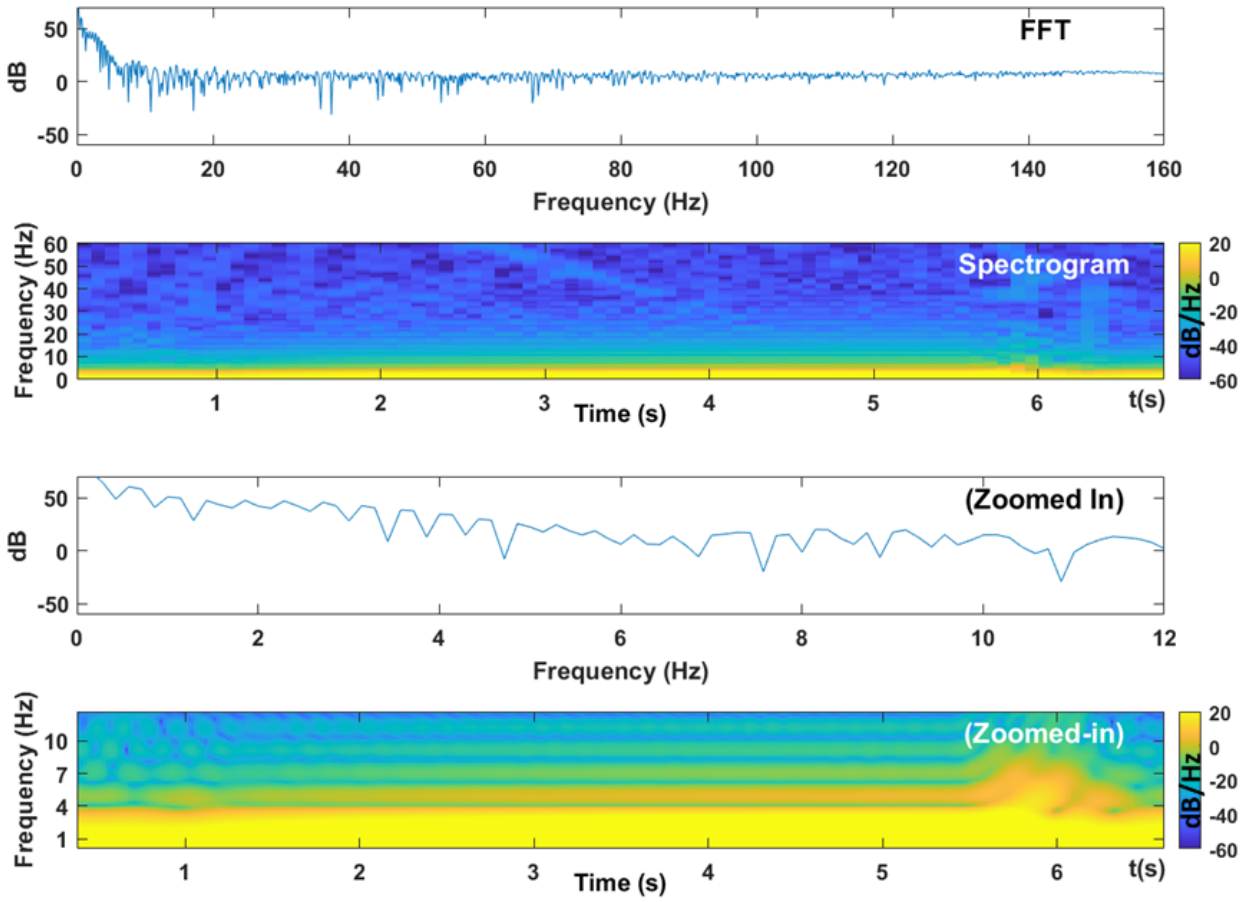

Figure 3.11: Pressure Frequency Analysis. FFT and spectrogram from an entire sample's pressure data in the constriction experiment. Everting tube exits constriction at about t = 5.8 s.

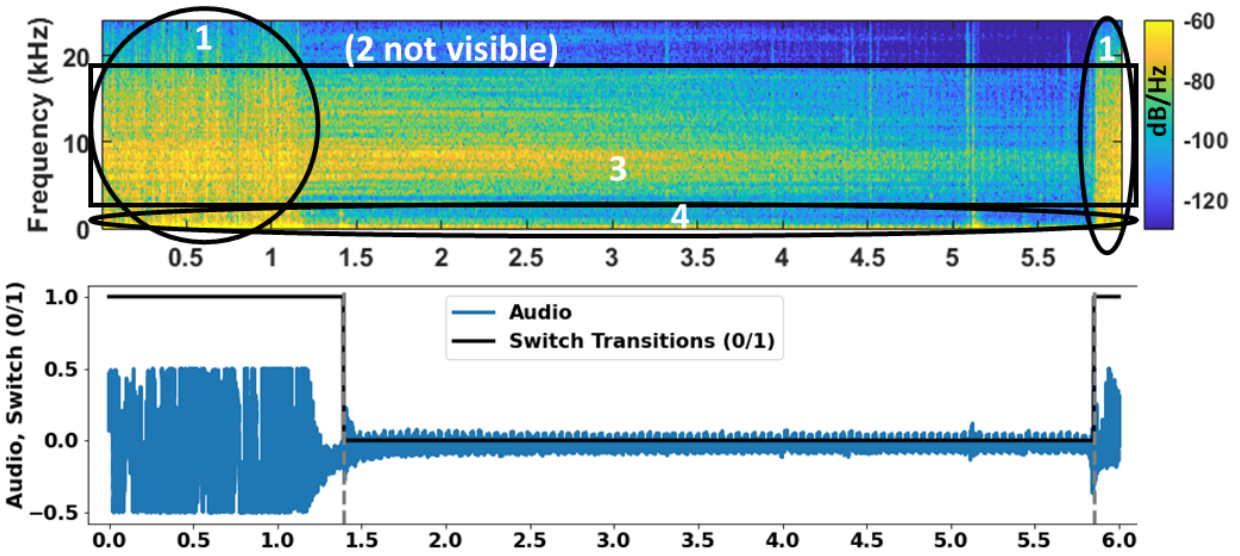

Figure 3.12: Audio from full constriction test. Top: Spectrogram. (1) Loud *Eversion into Tunnel*, (2) *Switch Clicked* which is not visible, (3) *Air Inflow* and (4) *Friction of Reel*. Bottom: Audio and switch data.

the constriction) it requires much higher everting pressure. Figure 3.7 shows these dramatic pressure rises and falls between transitions. Once the everting tube reaches the constriction at about t = 1.3 s, the pressure builds until it reaches a pressure required to pass the constriction. At about t = 5.8 s, the everting tube shoots through the constriction and transitions back into the larger tunnel, resulting in an abrupt drop in pressure. Using thresholding at 5.36 psi, the pressure thresholding algorithm (Fig 3.8, top) identified (TR1) within 0.986 s and identified (TR2) within 0.108 s (Fig 3.9, top). One threshold was used across the entire signal, but to optimize detection in future studies, this 5.36 psi threshold can be separated into two values and shifted lower for entering the constriction (TR2), and likewise, higher for exiting the constriction (TR2). Audio: In Figure 2.6, the everting tube in the larger tunnels generated louder sounds (faster speed), while in the constrictions sounds are quieter (slower speed). For example, when entering the constriction (TR1) at about t = 1.3 s, the audio immediately gets quieter. Using thresholding at 0.48, the audio thresholding algorithm (Fig 2.7, bottom) identified TR1 0.212 s early and TR2 0.002 s after (Fig 2.7, bottom). This

early identification (-0.212 s) indicates that the everting tube may momentarily be outside the constriction before gaining or building enough pressure to cross the threshold between the larger tunnel and the constriction (which then triggers the switch).

Like the previous experiment, we found pressure and audio signal thresholding can estimate when tunnel transitions occur. Specific to this experiment, we estimated transitions within 0.347 s (standard deviation of 0.321 s) using pressure signals, and -0.207 s (0.269 s) using audio signals. This suggests that audio data could sometimes indicate a transition into the constriction before it occurs. As stated above, this is likely because the everting tube is outside the constriction for a moment before gaining or building enough pressure to cross the threshold between the larger tunnel and the constriction (which then triggers the switch)). Note that a comparison of the proximal and distal transition data is insignificant in this experiment.

This experiment further supports that audio spectral analysis can classify sounds of everting tubes. Eversion sounds collected in Chapter 2 are distinguished and labeled in the overall full constriction test's spectrogram (Fig. 3.12) and help indicate when tunnel transitions occur. A larger tunnel segment causes faster eversion and louder LDPE plastic crinkling and louder reel movement, thus (1) (as labeled in Fig. 3.12) sections have more prominent eversion sounds. When prominent eversion sounds (1) cease ($t \sim 1$ s), the entering contriction (TR1) transition can be visually identified and when these broadband sounds begin ($t \sim 5.8$ s), the exiting constriction (TR2) transition can be visually identified. These TR1 and TR2 transitions line up with the switch transitions shown in the bottom of Fig. 3.12. Both (1) and (2) are broadband sounds, and are superimposed on one another, which would otherwise make them difficult to distinguish, but we know when switch clicking occurs from the limit switches ($t \sim 1.5$ s) so it is not necessary to always be able to distinguish it in the spectrogram. Note that all the FFTs reflect 140 Hz LPFs and HPFs used to separate the audio and pressure signals.

Chapter 4

EXPERIMENT COMPARISON

The alternating tunnels experiment in Chapter 2 tested if even a slight change in tunnel diameter was distinguishable in pressure and audio signal response. The constriction experiment in Chapter 3 tested if larger tunnel size differences produced more substantial pressure and audio signal responses. Recall, the cross-sectional area ratio of larger tunnel over smaller tunnel (or constriction) was 2.25 in the alternating tunnel experiment and 6.25 in the constriction experiment (2.25 vs 6.25). The alternating tunnels experiment showed distinguishable signal responses and the constriction experiment, with a larger diameter difference (2.858 cm v. 1.27 cm), produced more dramatic signal responses. Pressure differences were much more dramatic than in the alternating tunnel experiment (Figure 3.7 vs 2.6). Pressures reached about 8 psi in the constriction compared to 3 psi in the smaller tunnel in the alternating tunnel experiment. Given P1 is the average pressure in the larger tunnels and P2 is the the average pressure in the smaller tunnels (or constriction), the everting pressure differential (P2 / P1) was about 4x larger in the constriction experiment.

A precise data analysis showed a significant difference in audio between experiments. The 1.905 cm diameter tunnel sections averaged 0.07 amplitude while the 1.27 cm diameter tunnels sections averaged 0.03 amplitude across all samples. There was no significant difference in the larger tunnel's audio magnitude (0.49 amplitude), which is expected since they have the same diameter cross-section. These amplitude values were calculated from the average of audio magnitude overall while in the smaller (2.858 cm or 1.905 cm) or larger (2.858 cm) tunnel sections, according to switch data. Given A1 is the average audio in the smaller tunnels (or constriction) and A2 is the average audio in the larger tunnels, the audio differential (A2 / A1) is about 2.3x larger in the constriction experiment. Audio differences

between tunnels were increased in the constriction experiment. Note that these differences, while significant, are not seen by the naked eye in Figure 3.7 and the alternating tunnel experiment's corresponding Figure 2.6.

Chapter 5

CONCLUSION

The alternating tunnels and constriction experiments show unique signal responses in internal pressure and audio data from everting tubes. They also show distinguishable eversion sounds in their spectrograms. These studies are the first of their kind to study acoustic signals within everting tubes. This chapter discusses considerations, applications and future work to build on these findings.

5.1 Limitations

Only three different-sized tunnels were used and future studies should include more sizes. For the individual experiments, two different tunnels were used, with a smaller 2.25 and larger 6.25 cross-sectional area ratio (Experiment 1 and 2, respectively). This supports the assertion that different diameter tunnels cause distinguishable pressure and audio signals, even in tunnels/lumens with smaller size differences.

In this study, data were off-line and future studies should apply predictive, real-time algorithms in a causal manner. The thresholding algorithms were analyzed one transition at a time and will not work for the entire time span. For example, the pressure algorithm finds the initial threshold crossing and the audio algorithm finds the last peak (in an LS transition) or the first peak (in an SL transition).

Our recorded sounds depend in part on our experimental setup and will vary by configuration. For example, not all eversion configurations will use limit switches, a pressure vessel with a reel, or have tunnels/lumens with identical properties and echoing. The PVC tunnels may have prolonged duration of sounds in our spectrograms by echoing, and future studies may test this by comparing a click of the switch not in the tube.

Lastly, this experiment studied freely everting tubes and future studies should look at acoustic signals from controlled eversion, such as when a motor controls tubing release from the reel. Eversion control mechanisms will change pressure dynamics and might add or reduce noise and vibration.

5.2 Future Work

We calculated 95% of audio energy to lie below 8155 Hz (average from the audio FFTs). This suggests that, depending on the application, microphones can be sampled at 20 kHz instead of the consumer audio rate of 44kHz.

With additional experimentation, these pressure and audio sensing results could train deep learning models to classify eversion sounds. Eversion pressure and audio time signals can be classified, similar to research that has classified heartbeats signals on a deep neural network [12]. Eversion sounds can also be identified through image-analysis of their audio spectrograms, similar to work in speech recognition [13].

Techniques in this paper can be applied to other eversion scenarios to classify other environmental interactions, such as everting through curved tunnels of different radii. When introduced through a natural orifice like the esophagus, pressure signals could estimate the physiological state of the body, for example detecting pressure fluctuations imposed on the tube due to pulse and respiration.

In some medical applications, saline may be a more practical option than air to pressurize the everting tube. It has a faster speed of sound and has less damping, and could therefore extend sensing capabilities. Even so, some applications may be too noisy for meaningful audio signals. Fluid acoustic sensing could help in some archaeological applications with longer everting tubes that may not produce meaningful acoustic signals via air transmission [14].

Another promising future direction is active acoustic or electromagnetic sensing in which a pulse or other waveform can be applied at the proximal end of the tube and analysis of return echos, resonances, or wave variables could reveal interesting properties including

length and diameter variations.

Future studies can deploy everting tubes as sensors in hard-to-reach places. Everting tubes are already being studied in medical procedures such as breast cancer detection, brain surgery and colonoscopies [3, 4, 2]. Some of these hard-to-reach places such as the mammary glands, brain ventricles, and the colon, have environments that are not easily seen and are not safe for rigid probes. As the everting tube grows, acoustic sensing can help indicate what the environment looks like or if the tube is stuck.

Another medical example is emergency airway management. Recent research has investigated sending multi-material everting tubes into the trachea to seal the airway and restore oxygenation in sub/unconscious patients [1]. Acoustic signals could indicate when the everting tube leaves the trachea and enters the esophagus (the wrong tunnel), or if it gets stuck.

5.3 Conclusion

Everting tubes are good at getting to difficult places, but deploying sensors on distal parts of everted tubes is complicated. Our solution uses inexpensive sensors located in the base to measure or detect information about transient events. This has the promise to enrich many of the applications for which everted tubes have been proposed. Acoustic and pressure sensing from the base can gather navigation and environmental information, or beyond these existing applications, everting tubes can be deployed solely for the purpose of sensing. Our initial results demonstrate the potential that acoustic sensing capabilities will greatly assist applications of everting robots in unseen and hard-to-reach places.

BIBLIOGRAPHY

[1] J. Hwee, A. Lewis, R. A. Bly, K. S. Moe, and B. Hannaford, "An everting emergency airway device," in *2021 International Symposium on Medical Robotics (ISMR)*, 2021, pp. 1–7.

[2] A. Saxena, E. M. Pauli, R. S. Haluck, B. Fell, and J. Moore, "Tubular Locomotion and Positioning Using Tip Eversion for Endoscopy," *Journal of Medical Devices*, vol. 14, no. 2, 03 2020, 021004. [Online]. Available: https://doi.org/10.1115/1.4046433

[3] P. Berthet-Rayne, S. M. H. Sadati, G. Petrou, N. Patel, S. Giannarou, D. R. Leff, and C. Bergeles, "Mammobot: A miniature steerable soft growing robot for early breast cancer detection," *IEEE Robotics and Automation Letters*, vol. 6, no. 3, pp. 5056–5063, 2021.

[4] P. Slade, A. Gruebele, Z. Hammond, M. Raitor, A. M. Okamura, and E. W. Hawkes, "Design of a soft catheter for low-force and constrained surgery," in *2017 IEEE/RSJ International Conference on Intelligent Robots and Systems (IROS)*, 2017, pp. 174–180.

[5] E. W. Hawkes, L. H. Blumenschein, J. D. Greer, and A. M. Okamura, "A soft robot that navigates its environment through growth," *Science Robotics*, vol. 2, no. 8, p. eaan3028, 2017.

[6] L. H. Blumenschein, M. M. Coad, D. A. Haggerty, A. M. Okamura, and E. W. Hawkes, "Design, Modeling, Control, and Application of Everting Vine Robots," *Frontiers in Robotics and AI*, vol. 7, no. November, pp. 1–24, 2020.

[7] A. H. Camargo, J. N. Rubenstein, S. Sozen, B. D. Ershoff, and M. L. Stoller, "Novel everting urologic access sheath: Potential advantages of decreased cellular advancement," *Journal of Endourology*, vol. 20, no. 2, pp. 153–156, 2006, pMID: 16509804.

[8] J. N. Rubenstein, M. Garcia, A. H. Camargo, A. B. Joel, and M. L. Stoller, "Novel everting urologic access sheath: Decreased axial forces during insertion," *Journal of Endourology*, vol. 19, no. 10, pp. 1216–1220, 2005, pMID: 16359219.

[9] J. D. Greer, T. K. Morimoto, A. M. Okamura, and E. W. Hawkes, "A Soft, Steerable Continuum Robot That Grows via Tip Extension," *Soft Robotics*, vol. 6, no. 1, pp. 95–108, 2019. [Online]. Available: https://www.liebertpub.com/doi/10.1089/soro.2018.0034

[10] D. Brill and G. C. Gaunaurd, "Resonance theory of elastic waves ultrasonically scattered from an elastic sphere," *Journal of the Acoustical Society of America*, vol. 81, pp. 1–21, 1987.

[11] D. S. Drew, M. Devlin, E. Hawkes, and S. Follmer, "Acoustic communication and sensing for inflatable modular soft robots," 2021.

[12] S. Gao, Y. Zheng, and X. Guo, "Gated recurrent unit-based heart sound analysis for heart failure screening," *BioMedical Engineering OnLine*, vol. 19, 01 2020.

[13] A. N. Shewalkar, "Comparison of rnn, lstm and gru on speech recognition data," Ph.D. dissertation, North Dakota State University, 2018.

[14] M. M. Coad, L. H. Blumenschein, S. Cutler, J. A. Reyna Zepeda, N. D. Naclerio, H. El-Hussieny, U. Mehmood, J.-H. Ryu, E. W. Hawkes, and A. M. Okamura, "Vine robots: Design, teleoperation, and deployment for navigation and exploration," *IEEE Robotics Automation Magazine*, vol. 27, no. 3, pp. 120–132, 2020.